The Astrophysical Journal, 714:732–747, 2010 May 1 doi:10.1088/0004-637X/714/1/732

DISCOVERY OF A SUPERLUMINAL Fe K ECHO AT THE GALACTIC CENTER: THE GLORIOUS PAST OF Sgr A* PRESERVED BY MOLECULAR CLOUDS

G. Ponti[1,2], R. Terrier[1], A. Goldwurm[1,3], G. Belanger[4], and G. Trap[1,3]
[1] APC Université Paris 7 Denis Diderot, 75205 Paris Cedex 13, France; ponti@iasfbo.inaf.it
[2] School of Physics and Astronomy, University of Southampton, Highfield, Southampton, SO17 1BJ, UK
[3] Service d'Astrophysique/IRFU/DSM, CEA Saclay, Bat. 709, 91191 Gif-sur-Yvette Cedex, France
[4] ESA/ESAC, P.O. Box 78, 28691 Villanueva de la Cañada, Spain
Received 2009 December 21; accepted 2010 March 1; published 2010 April 14

ABSTRACT

We present the result of a study of the X-ray emission from the galactic center (GC) molecular clouds (MCs) within 15 arcmin from Sgr A*. We use *XMM-Newton* data (about 1.2 Ms of observation time) spanning about eight years. The MC spectra show all the features characteristic of reflection: (1) intense Fe Kα, with equivalent width of about 0.7–1 keV, and the associated Kβ line; (2) flat power-law continuum, and (3) a significant Fe K edge ($\tau \sim 0.1$–0.3). The diffuse low ionization Fe K emission follows the MC distribution, nevertheless not all MC are Fe K emitters. The long baseline monitoring allows the characterization of the temporal evolution of the MC emission. A complex pattern of variations is shown by the different MCs, with some having constant Fe K emission, some increasing, and some decreasing. In particular, we observe an apparent superluminal motion of a light front illuminating a molecular nebula. This might be due to a source outside the MC (such as Sgr A* or a bright and long outburst of a X-ray binary), though it cannot be due to low energy cosmic rays or a source located inside the cloud. We also observe a decrease of the X-ray emission from G0.11-0.11, behavior similar to that of Sgr B2. The line intensities, clouds dimensions, columns densities, and positions with respect to Sgr A* are consistent with being produced by the same Sgr A* flare. The required high luminosity (about 1.5×10^{39} erg s^{-1}) can hardly be produced by a binary system, while it is in agreement with a flare of Sgr A* fading about 100 years ago. The low intensity of the Fe K emission coming from the 50 and the 20 km s^{-1} MC places an upper limit of 10^{36} erg s^{-1} to the mean luminosity of Sgr A* in the last 60–90 years. The Fe K emission and variations from these MC might have been produced by a single flare of Sgr A*.

Key words: Galaxy: center – ISM: clouds – X-rays: ISM

Online-only material: color figures

1. INTRODUCTION

Sgr A*, the supermassive black hole (BH) at the center of the Milky Way, now radiates at a rate of about 8 orders of magnitude lower than the Eddington luminosity for its estimated mass of $M_{\rm BH} \sim 4 \times 10^6\ M_\odot$ (Schödel et al. 2002; Eisenhauer et al. 2003; Ghez et al. 2003, 2005; Gillessen et al. 2009). Such a low luminosity is difficult to reconcile with the dense environment that is present in the center of the Galaxy and has motivated the development of several radiatively inefficient accretion/ejection models (Melia & Falcke 2001). Although Sgr A* is known to display flares in X-rays (Baganoff et al. 2001; Goldwurm et al. 2003) and near-infrared (Genzel et al. 2003; Ghez et al. 2004), during which the X-ray intensity increases by factors up to 160 (Porquet et al. 2003) from the quiescent value, the bolometric luminosity still remains extremely low during these events compared to the Eddington one or even to the accretion power expected from the capture of stellar wind material from the nearby stars. On the other hand, one may wonder whether Sgr A* has always been so underluminous or if it experienced, in the past, long periods of high energy activity, that would make the massive BH of our Galaxy more similar, than it appears today, to typical low-luminosity active galactic nuclei (AGNs).

Indication of Sgr A* past activity can be sought in the interstellar medium surrounding the BH. Sunyaev et al. (1993) were the first to interpret the X-ray emission, seen with GRANAT to roughly follow the distribution of the molecular clouds (MCs) of the region, as scattering by the molecular material of emission from a past outburst of Sgr A* and predicted, at that time, a correlation of the X-ray fluorescent line of neutral iron with the MC. Koyama et al. (1996) with *ASCA* and Murakami et al. (2001a) with *Chandra* did in fact find such a correlation, particularly evident with the most massive MC complex of the region, Sgr B2, and proposed, using parameters derived from this cloud, that Sgr A* underwent, about 300 years ago, a major outburst of X-ray emission, with a luminosity of the order of few 10^{39} erg s^{-1}.

The fluorescence line at 6.4 keV (Kα) is produced by the extraction of an electron from the inner shell (K) of neutral or low-ionized iron atoms and the following electron transition from the second shell (L). Such line (actually a close doublet) is generally associated with another line (Kβ) due to the transition from the upper (M) level. Collisionally ionized iron atoms in a hot plasma preferentially produce lines in the 6.5–6.9 keV range, associated with a plasma continuum spectrum. Thus, the origin of the 6.4 keV line is most probably associated with either a large irradiation by photons having energies higher than 7.1 keV or by energetic particles, most probably electrons.

Diffuse X-ray (2–10 keV) emission in the galactic center (GC) region is complex and still under intense investigation (Park et al. 2004; Goldwurm 2008; Koyama et al. 2009) but it certainly consists of at least the following components: a uniformly distributed soft emission well described by a low temperature ($\approx$1 keV) plasma, a little less uniform but centrally peaked 6.7 keV line associated with continuum emission described by a hot (kT $\approx$ 7 keV) plasma model, and a clumpy 6.4 keV iron line component well correlated with molecular material. The soft component can be fully explained by the supernova (SN) activity of the region, while the origin of the other components is more uncertain. The interpretation of hot plasma emission for

the 6.7 keV line and associated hard component is problematic because such plasma cannot be confined in the region and its regeneration would require a too large amount of energy (but see Belmont & Tagger 2006 for a heating mechanism of a helium dominated hot plasma at the GC). An alternative is that the hot component may contain an important contribution from faint sources. This interpretation is supported by the similarity in the X-ray and near-infrared surface brightness distribution (Revnivtsev et al. 2006) and by the large fraction of weak point sources in the population that the *Chandra* deep survey of the GC unveiled (Muno et al. 2004; Revnivtsev et al. 2007). For the 6.4 keV component, two models of emission are competing: the reflection model quoted above (Sunyaev & Churazov 1998), and one that attributes the 6.4 keV emission to low energy particles, most probably electrons (Valinia et al. 2000; Yusef-Zadeh et al. 2002a, 2007). In the frame of the latter model, the impact by low energy protons (Dogiel et al. 2009) or by fast moving SN ejecta (Bykov 2003) with neutral material have also been considered.

This emission line has been detected in other, but not all, MCs of the central region (Murakami et al. 2001b; Yusef-Zadeh et al. 2002; Nakajima et al. 2009), for which a reflection from single Sgr A* event interpretation is more problematic and for some of which has also been found a correlation with non-thermal radio filaments, indicating local particle acceleration (Yusef-Zadeh et al. 2007).

On the other hand, the detection of hard X-ray emission up to 100 keV from Sgr B2 obtained with the Integral observatory by Revnivtsev et al. (2004) supports the reflection nebula interpretation. These authors also demonstrated that the emission line intensity was constant until about 2000 and therefore that the original outburst must have lasted at least 10 years. However, the most convincing evidence that supports the photon-ionization model from an external source, comes now from the recent detections of variability of the line and continuum emission, a signature predicted and modeled in detail by Sunyaev & Churazov (1998). Up to now two different claims of variability detection have been published. Muno et al. (2007) observed variation in the continuum (not in the line emission) flux and morphology from two 6.4 keV nebulae at about 6 arcmin from Sgr A*. Then using data from several satellites (*ASCA*, *Chandra*, *XMM-Newton*, and *Suzaku*), Koyama et al. (2008) and Inui et al. (2009) showed that the Sgr B2 6.4 keV line emission is changing in a way that it would be produced by a wave front passing through the different components of the Sgr B2 complex.

Maybe the more compelling evidence, up to now, is the discovery of time evolution of the hard X-ray emission from Sgr B2 observed over seven years by the same instrument on the *INTEGRAL* satellite (Terrier et al. 2010). Indeed the evolution of the hard X-ray emission of Sgr B2 is best explained by an X-ray reflection nebula scenario in which the fading of the reflection component (for the first time measured in the Compton hump region) is due to the propagation of the decay part of the outburst and rules out competing models based on irradiation by low energy cosmic ray electrons.

However, Sgr B2 is quite a special object and one may wonder whether the reflection nebula model works only for this cloud or if it holds for the other 6.4 keV features of the region. If the origin of the scattered emission is external to the cloud, signatures should be seen elsewhere. Sgr B2 is indeed not the only MC close to Sgr A*. The supermassive BH sits on the middle of the Central Molecular Zone (CMZ; Morris & Serabyn 1996), a condensation of MCs right in the center of the Galaxy. The detailed study of this region can therefore validate the reflection model and even narrate the past history of Sgr A* emission (Sunyaev et al. 1993; Sunyaev & Churazov 1998; Cramphorn & Sunyaev 2002). Moreover, the light front due to a major flare may be used as a tool to scan the distribution of the MC material in the CMZ.

Table 1
Progressive Observation Number, Progressive Number of the Summed Observations, Observation Date, Total Observation Time, Cleaned Exposure (EPIC-pn), Observation ID, and Filter of the *XMM-Newton* Observations Pointed Toward Sgr A*

N	Gr	Date	Time (ks)	Expo (ks)	Obs. ID	Filter
1	1	2001 Sep 4	27.7	18.3	0112972101	M
2	1	2002 Oct 3	17.3	8.6	0111350301	T
3	2	2004 Mar 28	133.0	17.3	0202670501	M
4	2	2004 Mar 30	134.4	35.4	0202670601	M
5	3	2004 Aug 31	135.2	84.3	0202670701	M
6	3	2004 Sep 2	135.2	94.6	0202670801	M
7	4	2007 Mar 30	35.2	57.2	0402430701	M
8	4	2007 Apr 1	105.4	39.4	0402430301	M
9	4	2007 Apr 3	105.8	25.3	0402430401	M
10	5	2008 Mar 23	105.7	72.4	0505670101	M
11	6	2009 Apr 1	39.9	28.8	0554750401	M
12	6	2009 Apr 3	44.3	35.5	0554750501	M
13	6	2009 Apr 5	39.1	27.8	0554750601	M

The main focus of this work is the study of the X-ray emission from the MCs located around Sgr A* using the eight-year Sgr A* monitoring program carried out with the *XMM-Newton* satellite.

In Section 2, the different observations and data reduction are presented. Section 3 shows the GC images in the Fe Kα band and the analysis of the CS maps, with the aim to correlate the Fe K emission with the MC disposition, so that we can infer the location/distribution and column density of the different MCs within the *XMM-Newton* field of view. Section 4 presents the mean spectra from the different regions selected through the CS maps. Section 5 shows the time evolution of the Fe K emission from the MC. Section 6 shows the discovery of a superluminal echo in a X-ray reflecting nebula. In Section 7, the results are discussed, in particular in Subsection 7.2 the possibility that all MCs are illuminated by a single flare from Sgr A* is discussed. The conclusions are summarized in Section 8.

2. OBSERVATION AND DATA REDUCTION

Sgr A* and the MCs in its immediate proximity, i.e., within a circle of 15 arcmin radius, have been observed up to now 13 times by *XMM-Newton*, spanning a period of eight years. Table 1 shows the observation dates, exposures, and IDs of the different pointings, all directed toward Sgr A*. Photon list files were created from the original Observation Data Files (ODF) using the *XMM-Newton* Science Analysis Software (SAS) version 7.1.0. The EPIC pn and both MOS cameras were operated in full-frame and large-window mode, respectively. The loss of CCD6 in the EPIC-MOS1 camera after 2005 March 9 (most probably due to a micro-meteoroid; Abbey et al. 2006), prevents us from extracting MC spectra from the corresponding region during the 2007, 2008, and 2009 observations.

Most of the observations were affected by strong particle background flares. In order to reduce such contamination, we visually inspected all the EPIC-pn light curves and cut the periods during which the pn full field of view 10–12 keV count rate is higher than about 2 counts s^{-1}. This severely reduced the exposure time (see Table 1), but it provides cleaned data sets, where the impact of the particle background is negligible.

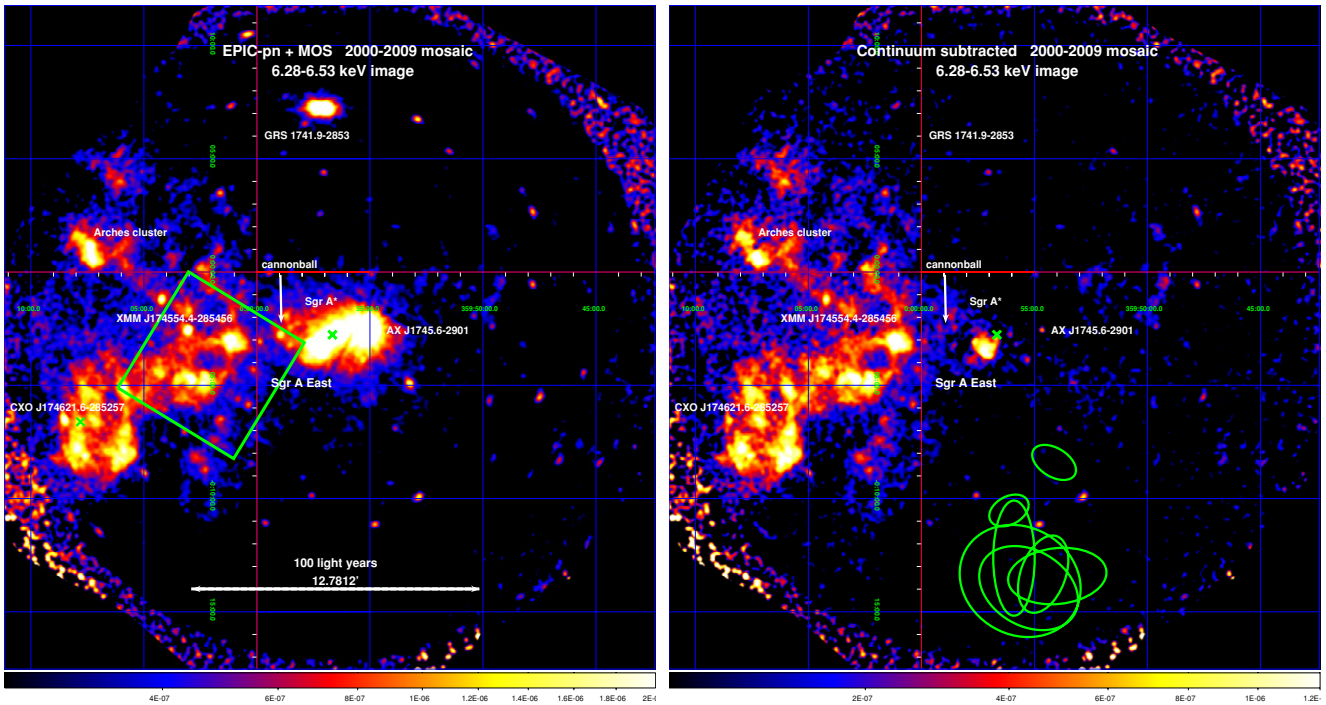

Figure 1. Left panel: mosaic EPIC-pn + MOS images of all the *XMM-Newton* observation between 2000 and 2009. The events are selected between 6.28 and 6.53 keV, the energy band that contains the neutral Fe K emission line. The stronger features are due to transient point sources with strong continuum and weak Fe Kα lines. The green square shows the region studied by Muno et al. (2007) and shown in their Figure 2. Right panel: continuum subtracted Fe K image assuming an absorbed power-law continuum shape with spectral index of $\Gamma = 2$. Most of the contribution due to point sources is removed. Strong diffuse Fe Kα emission is present close to the Galactic plane east of Sgr A*. The green ellipses at low Galactic latitude show the background extraction regions. Galactic north is up.

We then select the same good time intervals for the EPIC-MOS camera. For both pn and MOS cameras, single and double events have been selected. For spectra we selected FLAG zero events only, while the expression (FLAG & 0XFB002C) == 0 has been used to extract photons to produce images.

For the spectra, source plus background photons were extracted from the regions shown in Figure 2. The background spectrum was extracted from regions south of the Galactic plane where the impact of point sources is minimal (see the right panel of Figure 1). With the SAS commands ARFGEN and RMFGEN ancillary and response files were created. The source and background spectra and response files are added with the FTOOL MATHPHA. In the subsequent spectral analysis, source spectra were grouped such that each bin contained at least 30 counts and errors are purely statistical and quoted at the 90 percent confidence level ($\Delta\chi^2 = 2.7$ for one interesting parameter), if not otherwise specified. Spectral fitting was performed using XSPEC 12.4.0.

All the images have been first corrected for out of time events (produced with the SAS command and then subtracted using the FTOOLS command FARITH). These images have been then merged with the SAS command EMOSAIC. The exposure maps were calculated with the command EEXPMAP and then used to normalize the images. With DS9 a Gaussian smoothing, with a kernel radius of 10 pixels, has been applied to the resulting images that have 1 arcsec pixels.

3. SPATIAL DISTRIBUTION OF THE Fe Kα DIFFUSE EMISSION

The left panel of Figure 1 shows an image of the entire EPIC field of view in the 6.28–6.53 keV energy band. This band contains the Kα fluorescence line of the neutral or low-ionization Fe atoms, that peaks at 6.4 keV. The image is the result of the mosaic of the images of each observation and the three cameras aboard *XMM-Newton*. The stronger features are due to transient point sources with strong continua and with only weak 6.4 keV lines. To subtract the emission from these sources and to disentangle the emission due to the Fe Kα line, we first computed the continuum emission image in the 4.5–6.28 keV band, then assumed that the continuum spectral shape is described by an absorbed power-law shape with spectral index $\Gamma = 2$. This allowed us to calculate the continuum contribution underlying the Fe K line emission and thus subtract it after properly rescaling the continuum image (a factor of 0.106 has been used). The right panel of Figure 1 shows that, once the continuum is properly subtracted, the emission from AX J1745.6-2901, GRS 1741.9-2853, XMM J174554.4-285456, the Arches cluster, the cannonball, CXO J174621-285257, and the other point sources is correctly subtracted. Only Sgr A East leaves a clear residual, because of its strong 6.7 keV line, contaminating also the Fe Kα region with its wings.

If the latter region is ignored, one can easily see that a strong, diffuse, Fe Kα emission at $\sim$6.4 keV is present in the region, and that it is distributed along the Galactic plane in a non-uniform way with several hot spots, more numerous and prominent on the galactic east side of Sgr A*. Figure 2 shows an enlargement of this region. As already well known, a similar general asymmetry is present in the MC distribution, suggesting a strong link between the 6.4 keV hot spots and MC complexes. We therefore perform an accurate study of the correlation between the bright 6.4 keV line structures and the molecular matter distribution, using public data of molecular line emission of the GC region.

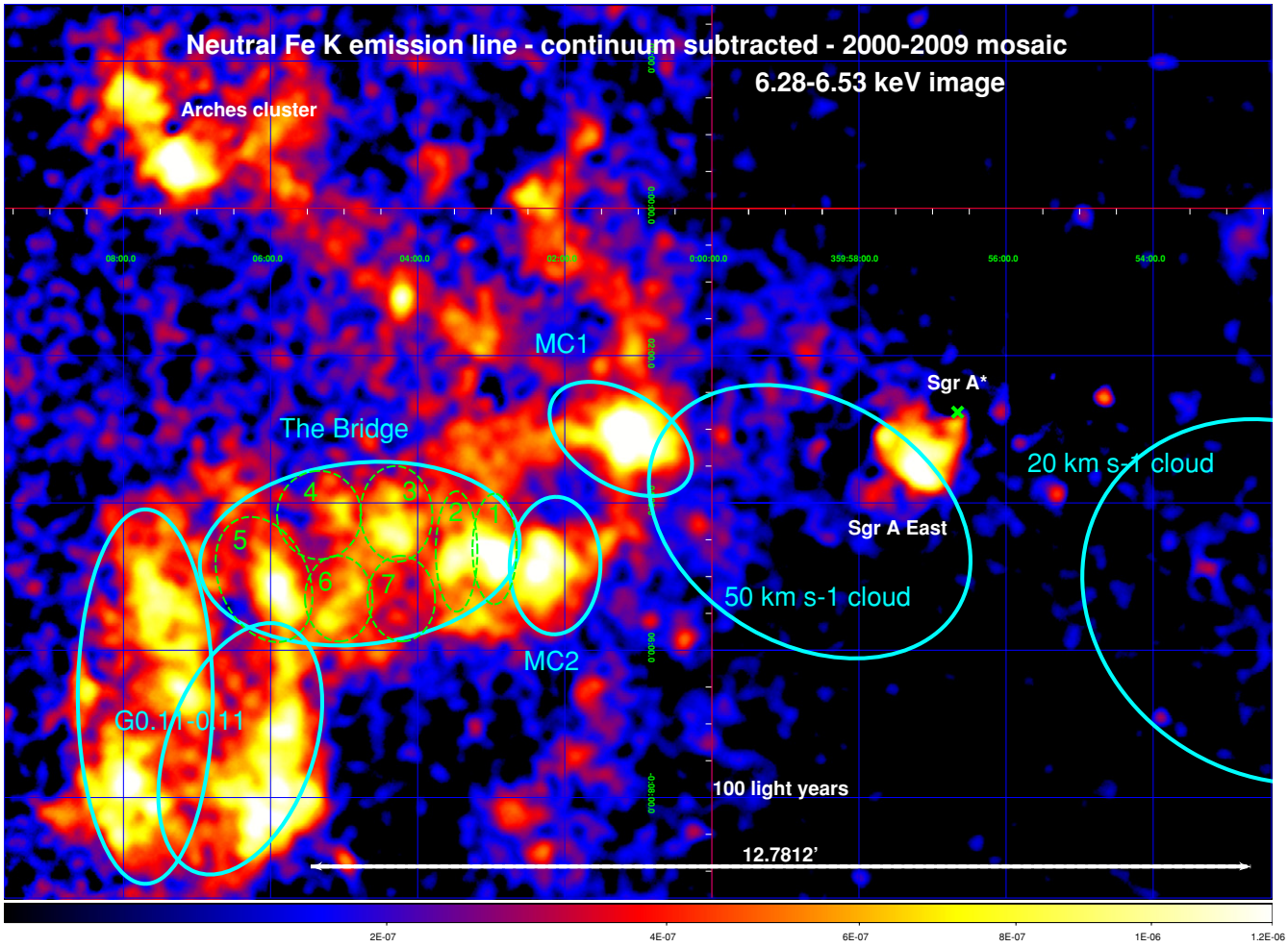

Figure 2. Enlargement of the Fe K, continuum-subtracted intensity map. The solid light blue ellipses show the regions selected through the study of the CS maps and the comparison with the Fe K map. These should indicate and separate the emission from the different MCs. The corresponding background regions have been selected from an area at high latitude, south of the GC (see the right panel of Figure 1). The green dashed ellipses show the subdivision of the bridge area into smaller regions.

3.1. Comparison with Molecular CS Emission

The molecular gas of the Galaxy is strongly concentrated within the central few hundred light years (Bally et al. 1987; Tsuboi et al. 1999) in the so-called CMZ. About 10% of the molecular gas of the Galaxy is contained in this region (the CMZ has an estimated mass of several $\times 10^7 M_\odot$) and it is less than 1% of the Galaxy volume. MCs in the CMZ are known to have a higher density relative to the Galactic norm and for these reasons they are better depicted through high-density tracers like CS (Bally et al. 1987; Tsuboi et al. 1999), NH_3 (Gusten et al. 1981; Morris et al. 1983), and HCN (Fukui et al. 1977; Jackson et al. 1996) lines than the CO line, usually employed for the rest of the Galaxy. To map the location of the more dense and compact MCs, we use the CS $J = 1$–0 data-cube provided by Tsuboi et al. (1999). Large velocity gradients are experienced by the molecular gas within the CMZ. Most probably, the clouds are not in Keplerian motion around the central BH. In this region, in fact, the mass concentration dominating the gravitational potential is given by stars that appear to be distributed in a bar. Because of the resulting non-circular motions, it is not possible to uniquely infer the distance to an MC from its position in the sky and its velocity along the line of sight.

Several authors have attempted to provide a three-dimensional distribution of the molecular material in the CMZ using different tools to reconstruct the MC position along the line of sight. Vollmer et al. (2003) observed a population of infrared point sources in the GC and, assuming an axisymmetric distribution, they estimated the MC position through their observed extinction (see also Becklin et al. 1982; Glass et al. 1987). Nevertheless, this technique provides only a very rough estimate of the distance. Up to now it has been possible to apply parallax measurements only to Sgr B2 (Reid et al. 2009). Sawada et al. (2004) proposed a method based on the comparison between emission and absorption in the radio band and applied it to the entire CMZ. Ryu et al. (2009) proposed a method based on the X-ray absorption toward the Sgr B region. Nevertheless, these interesting studies do not have enough resolution to measure the line-of-sight position of a single MC within the CMZ. On the other hand, single or spatially connected MC structures should have similar velocities. Selecting the MC emission in different velocity ranges, it might be possible to separate the MC distribution along the line of sight.

The different panels of Figure 3 show the CS sky images corresponding to the EPIC-pn field (lower-right panel) integrated over different velocity ranges, in order to differentiate the various MCs. The intensity of CS emission (directly correlated with the MC mass when, as in the present case, CS auto-absorption does not occur) is shown in Figure 3 with the same linear color scale going from $T_{\rm MB} = 2.85$ K km s^{-1} (in order to select

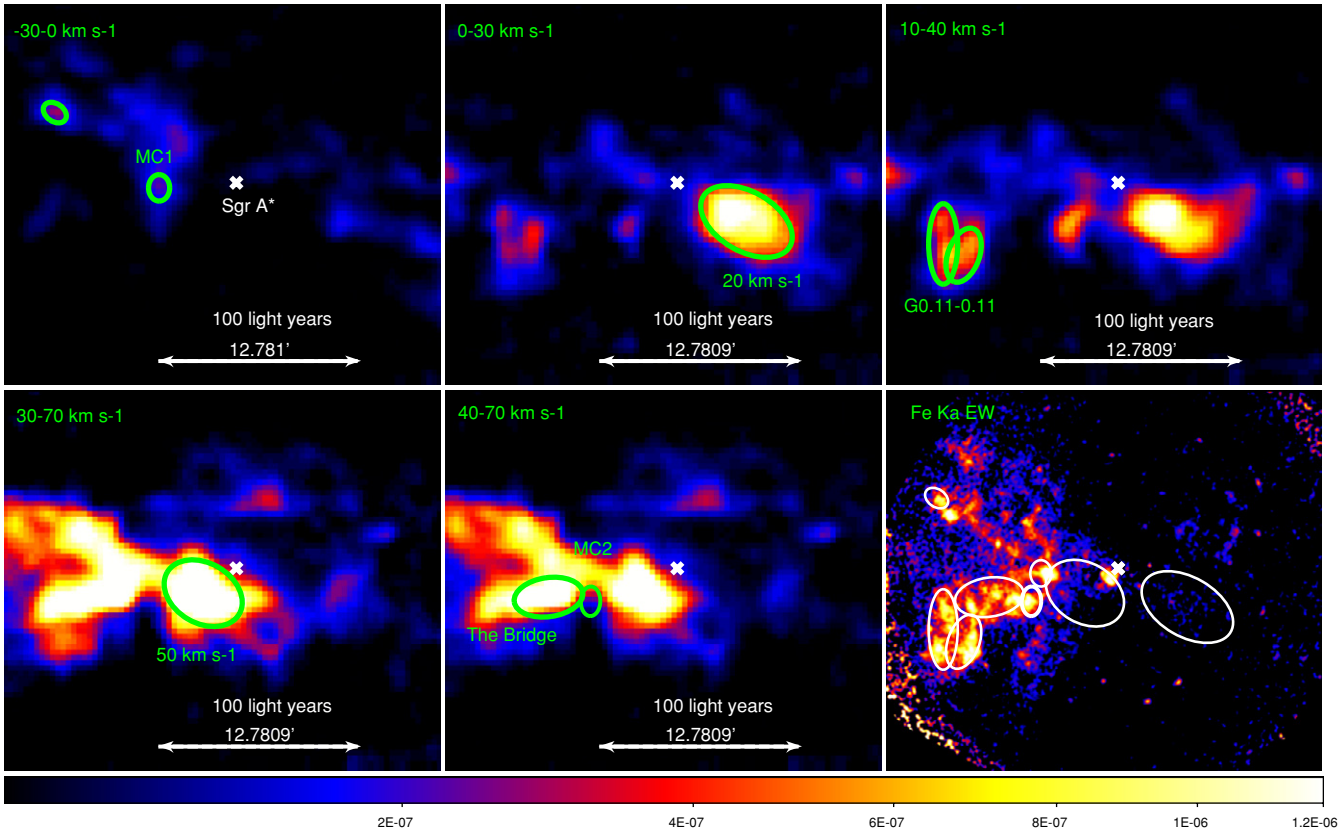

Figure 3. CS maps from Tsuboi et al. (1999). The different images are integrated over different velocity ranges to differentiate the coherent structures and try to separate emission coming from different regions along the line of sight. Lower right panel: continuum-subtracted Fe Kα image.

only massive MCs) to 60 K km s^{-1}. Using the formula from Tsuboi et al. (1999): $n_H = \frac{7.5\times10^{11}\times T_{\rm ex}\times\int T_{\rm MB}dv}{10^{-8}}$ cm^{-2}; we derive, for those values, column densities equal to $n_H = 4.3 \times 10^{21}$ and 9×10^{22} cm^{-1}, respectively (assuming abundance X(CS) $= 10^{-8}$; Irvine et al. 1987; and excitation temperature of CS of $T_{\rm ex} = 20$ K[5]). Table 2 shows the physical parameters of the different MCs that we identified as measured from the X-ray and CS data. The second column shows the column density (n_H), the third the mean radius (R), the fourth the projected distance from Sgr A* (D_p), and the fifth the line-of-sight distance with respect to the plane of Sgr A* ($D_{\rm los}$). To calculate the MC column densities from the CS maps we summed the CS emission in the −30–0, 0–30, 30–70 and 40–70 km s^{-1} velocity ranges for the MC1, 20 km s^{-1}, 50 km s^{-1} and the bridge MC, respectively. No major massive MC is observed characterized by either velocities lower than −30 km s^{-1}, or higher than 70 km s^{-1}, thus we do not show the corresponding images.

Figure 3 shows that the same asymmetry present in the Fe K line intensity image is present also in the MC distribution.

Table 2
MC Physical Parameters

Name	n_H (cm^{-2})	R (pc)	D_p (pc)	$D_{\rm los}$ (pc)	$\Delta V_{\rm LSR}$ (km s^{-1})
Bridge	9×10^{22}[a]	1.6	18	60[b]	40–70
G0.11-0	2×10^{22}[c]	3.7	25	17[b]	10–40
50 km s^{-1}	9×10^{22}[a]	4	5	5–10	30–70
MC1	4×10^{22}[a]	1.8	12	50[b]	−30–0
MC2	$<2 \times 10^{22}$[a]	1.8	14	<35[b]	
Sgr B2	8×10^{23}	7	100	−130[d]	

Notes. MC column density (n_H); radius (R); projected distance from Sgr A* (D_p); distance along the line of sight ($D_{\rm los}$) with respect to the plane of Sgr A* (negative values indicate objects closer to us than Sgr A*); CS integration velocity range ($\Delta V_{\rm LSR}$).
[a] Column density inferred from the CS maps of Tsuboi et al. (1999).
[b] Value estimated assuming that the MC is illuminated by the same flare illuminating Sgr B2.
[c] Amo-Baladrón et al. (2009).
[d] Reid et al. (2009).

Moreover, the more massive MC in the EPIC field of view are the 20 and 50 km s^{-1} MCs. They are located within 10–20 pc from the supermassive BH (Coil et al. 2000), their position with respect to Sgr A* is well known because of the physical interactions between these MC and Sgr East. The two MCs have velocities between 0–30 km s^{-1} and 30–70 km s^{-1}, respectively (see the middle upper and left lower panels of Figure 3).

Another well studied and massive MC in the field of view is G0.11-0.11 (Handa et al. 2006; Amo-Baladrón et al. 2009).

[5] Tsuboi et al. (1999) assume in their calculations an excitation temperature between 30 and 70 K, following the temperature measurements of the MCs in the GC (Gusten et al. 1981; Morris et al. 1983; Armstrong & Barrett 1985; Güsten 1989). Nevertheless, several authors studying ammonia and SiO lines show that these lines are subthermally excited for typical MCs within the CMZ (Gusten et al. 1981; Morris et al. 1983; Amo-Baladrón et al. 2009). In particular, Amo-Baladrón et al. (2009) calculate the column densities of several MCs in Sgr A, through the detailed measurement of the SiO excitation temperature, performed with a LVG excitation code. From these values it is possible to deduce the equivalent CS excitation temperature $T_{\rm ex}$ that results to be between 10 and 15 K. We thus assume a $T_{\rm ex}$ of 20 K, a compromise between these values and the minimum value considered by Tsuboi et al. (1999).

It appears in the velocity range between 10 and 40 km s^{-1} (see the upper right panel of Figure 3). Its shape is not easily reproducible by a single ellipsoid, thus we combine two ellipses to define it.

Two other bright Fe K spots appear in the X-ray image. Muno et al. (2007), analyzing the *Chandra* data (see the green square in the left panel of Figure 1 that corresponds to the region studied by Muno et al. 2007), already studied these two Fe K bright regions and indicated as features 1 and 2 (see Figure 2 of Muno et al. 2007). We keep the same name calling them MC1 and MC2. Scanning the CS maps, we find a possible counterpart for MC1 in the velocity range between −30 and 0 km s^{-1} (see the upper left panel of Figure 3), while we do not see a clear counterpart for MC2. For this reason we can place only an upper limit to its column density (see Table 2). The ammonia and CO emission from MC1 has been studied by Armstrong & Barrett (1985), calling it M0.02-0.05. The association of MC1 with the CMZ is still unclear. In fact, although the column density and temperature of this feature are typical of the CMZ, Amo-Baladrón et al. (2009) show SiO velocities for this cloud between −12.5 and −22.5 km s^{-1}. These velocities are consistent with the ones observed in the Galactic disk, but the linewidths seem to be broad, characteristic of the GC.

In the range between 40 and 70 km s^{-1} (see the lower middle panel of Figure 3) an intense structure appears in the CS maps with a reversed V shape. The horizontal branch spatially corresponds to strong low-ionization Fe K emission, while weaker emission is measured at the position of the vertical branch (see the lower right panel of Figure 3). The horizontal branch appears just east of the location of the 50 km s^{-1} MC and reaches the location of G0.11-0.11 (the branch and G0.11-0.11 appear in different velocity ranges, suggesting that these are not interacting, being at different distances along the line of sight). This feature appears like a unique structure of molecular gas, clearly more extended in the longitudinal direction. For this reason and in order not to confuse the reader with terms already used to indicate other famous structures in the GC, we call it (as Armstrong & Barrett 1985; Sakano et al. 2006) "the bridge." We note that in Figure 2 the bridge seems to further extend to the west without discontinuity into region MC2. Nevertheless the CS maps show a clear transition with the bridge ending before MC2. Thus the bridge and MC2 seem to be two separate MC structures.

We also mention that a bright spot in the upper left side of the X-ray image has a molecular counterpart. This region is associated to the Arches cluster and has been already studied using *XMM-Newton* and *Chandra* data (Yusef-Zadeh et al. 2002; Sakano et al. 2004; Wang et al. 2006). We will not, therefore, discuss this feature further in this paper.

In summary, the comparison between Fe K and CS emission shows a strong correlation between the two. In particular, we observe that MC emission is present wherever Fe Kα emission is bright; on the other hand, massive molecular complexes are present without associated Fe K emission. The solid green ellipses in Figure 2 show the selected regions from which the X-ray spectra will be extracted. The bigger region (the so-called "bridge") has also been subdivided into further, smaller areas (shown in dashed light blue in Figure 2) that will be used to perform time-resolved spectral analysis. We also note that Figure 2 shows other regions of diffuse Fe K emission. A more detailed study of this fainter component and its association to MC is deferred to a later work.

4. AVERAGE SPECTRAL CHARACTERISTIC OF MC

We compute the spectra of the different MC regions, delimited by the solid green ellipses in Figure 2. We then add all the spectra and response files with the FTOOL MATHPHA, keeping the different instruments separated. We use local background spectra (with the same extraction area as for the respective MC region) from positions at high Galactic latitude south of Sgr A*, within the same field of view (see the right panel of Figure 1). The subtraction of local background spectra almost completely removes the contribution due to the hard component of the X-ray diffuse emission (see Figure 4), including the 6.7 keV line (Revnivtsev et al. 2009), this latter being almost completely uniform on these angular scales. It also removes part of the emission from the low temperature (about 1 keV) plasma. However, residual soft lines appear in the X-ray spectra of the different MCs. For this reason we present the results of the spectral analysis considering only the 4–8 keV band. However, similar results are obtained considering the entire band (2–10 keV), once the contribution due to a low temperature plasma is considered to fit the low energy band.

As examples of MC emission, Figure 4 shows the X-ray spectrum of G0.11-0.11 and the bridge. The strongest spectral features are: (1) the neutral-low ionized Fe Kα line and the associated Fe Kβ; (2) a power-law continuum absorbed by neutral material; (3) an Fe K edge; and (4) a residual ionized Fe K emission (the line is almost completely removed with the subtraction of the local background). We thus fit the data with a phenomenological model given by the XSPEC model: WABS*(APEC+EDGE*(POWER-LAW+GAUS+GAUS)). Table 3 shows the best fit results of the mean spectra of the different MCs. The Fe K edge energy is fixed at 7.1 keV, the Fe K β emission energy fixed at 7.06 keV (as in Ponti et al. 2009), its width fixed to that of Fe Kα and its intensity tied to that of Fe Kα in order to keep a ratio $\beta/\alpha = 0.15$. We also assume Solar abundance (Grevesse & Anders 1989) for the emitting material and fix the temperature of the thermal (APEC) component to 6.5 keV (Koyama et al. 2007).

We observe (see Table 3) that the line energy is, in about all MCs, $E = 6.410 \pm 0.002$ keV, a value higher than the expected Fe Kα emission from neutral iron; nevertheless, once the systematic uncertainties are considered, it becomes consistent with emission from neutral Fe.[6] Also the line width is statistically not consistent with 0, being of the order of $\sigma \sim$ 20–30 eV. However, the lines are not significantly broad when the systematic uncertainties are considered (Guainazzi et al. 2010; de Grandi & Molendi 2009; Molendi & Gastaldello 2009).[7]

The Fe K line has equivalent width (EW) between ∼0.7 and 1 keV above the total observed continuum. Such high EW are

[6] The observed energy corresponds to emission from Fe XII–XIV (House 1969) that, assuming photo-ionization, would correspond to an ionization factor of about log(ξ)=1–1.5 erg cm s^{-1} (Makishima 1986). Nevertheless, we note that the calibration of the absolute energy scale of the EPIC instruments is known within 10 eV (CAL-TN-0018), thus the observed energy is still consistent with emission from neutral iron. The high value of the energy of the Fe K emission might be induced by the periods of high soft proton activities occurring during the observation (see Table 1). In fact, when the MOS data alone are considered (that have absolute energy scale uncertainty of 5 eV only) the Fe K energy results to be $E_{\rm FeK} = 6.405 \pm 0.005$ keV.

[7] Fitting simultaneously EPIC-pn and MOS data, we obtain line widths of the order of 20–30 eV. On the other hand, upper limits of 9 eV are obtained when the MOS data only are considered, while a width of 39 ± 5 eV is obtained fitting EPIC-pn data only. Moreover, following Guainazzi et al. (2010) we checked that (analyzing CALCLOSED observations) the calibration lines measured by the EPIC-pn camera have systematic width of the order of 20–40 eV. The measured Fe K lines are thus consistent with being narrow.

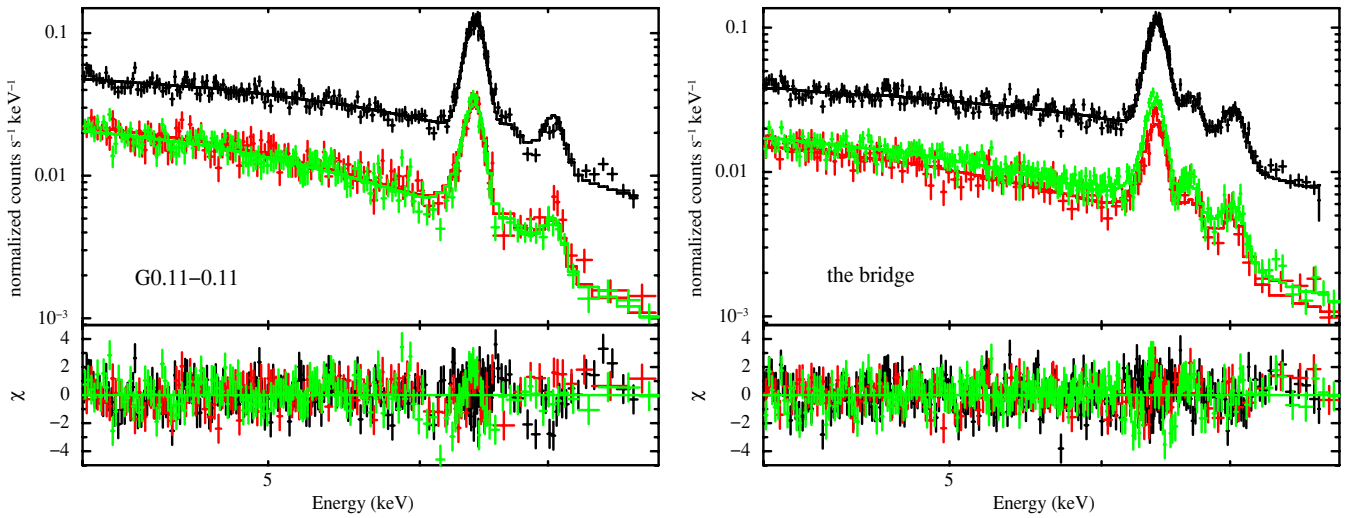

Figure 4. X-ray spectrum of G0.11-0.11 and the bridge. EPIC-pn in black, MOS1 in red and MOS2 in green. Clearly evident are the Fe Kα+β lines, the Fe K edge, the flat power-law continuum.

(A color version of this figure is available in the online journal.)

Table 3
Best Fit Results of the Fit of the Mean Spectra of the Different MCs

Model: wabs × (apec + edge × (power-law + Gaus + Gaus))									
Name	nh 10^{22} (cm^{-2})	τ	E (keV)	σ (eV)	$Norm_{Ga}$ 10^{-5} (ph. cm^{-2} s^{-1})	Γ	$Norm_{pl}$ 10^{-5} (ph. keV^{-1} cm^{-2} s^{-1})	EW (eV)	χ^2/dof
Bridge	4 ± 3	0.26 ± 0.12	6.409 ± 0.002[a]	28 ± 4[b]	$4.7^{+0.3}_{-0.2}$	$1.0^{+0.4}_{-0.3}$	26^{+22}_{-13}	750	1175.1/1121
G0.11-0.11	7 ± 4	$0.03^{+0.11}_{-0.03}$	6.411 ± 0.002	28 ± 5	7.5 ± 0.5	$1.9^{+0.3}_{-0.4}$	250^{+200}_{-130}	955	1302.0/1175
MC1	10^{+1}_{-2}	0.32 ± 0.07	6.410 ± 0.005	<18	$1.87^{+0.18}_{-0.06}$	$0.8^{+0.4}_{-0.5}$	10^{+10}_{-5}	684	780.3/780
MC2	5^{+5}_{-4}	$0.36^{+0.2}_{-0.15}$	6.411 ± 0.004	30^{+7}_{-10}	$0.98^{+0.17}_{-0.09}$	$0.9^{+0.1}_{-0.5}$	$6.3^{+0.5}_{-2}$	715	755.1/615
Model: wabs × (power law + apec + pexrav+ Gaus + Gaus)									
name	nh		E	σ	$norm_{Ga}$	Γ	$norm_{pl}$		χ^2/dof
Bridge	4 ± 3		6.409 ± 0.002	26 ± 5	4.6 ± 0.2	2.1 ± 0.1	78^{+55}_{-34}		1179.7/1122
G0.11-0.11	6^{+2}_{-3}		6.411 ± 0.002	27 ± 5	$7.1^{+0.4}_{-0.3}$	2.4 ± 0.2	420^{+160}_{-130}		1309.5/1176
MC1	9^{+2}_{-4}		6.410 ± 0.005	<20	1.9 ± 0.07	1.9 ± 0.1	28^{+24}_{-15}		781.8/781
MC2	8^{+6}_{-5}		6.409 ± 0.004	23 ± 10	1.2 ± 0.1	2.1 ± 0.2	35^{+18}_{-10}		760.0/615

Notes. EPIC-pn and MOS data are fitted simultaneously. Upper panel: fit with the phenomenological model. Lower panel: fit including the reflection continuum. Column densities are in units of 10^{22} cm^{-2}; Fe Kα normalization in units of 10^{-5} ph $cm^{-2}s^{-1}$; power-law normalization in units of 10^{-5} ph. keV^{-1} cm^{-2} s^{-1} at 1 keV.

[a] Please note that the calibration of the absolute energy scale of the EPIC instruments is known within 10 eV uncertainty (CAL-TN-0018), higher than the Fe Kα statistical uncertainty.

[b] The EPIC-pn and MOS energy resolution at the Fe K energy is of the order of $\sigma \sim 60$ eV.

in agreement with a reflection origin for the line and they imply a minor contribution from other sources of continuum different from reflection. The power-law continuum is observed to be extremely flat with a spectral index between about $\Gamma \sim 0.6$ and 1.7. In the majority of the MC, the Fe K edge is detected with high significance (between 65% and 99.9%).

We thus add to the model a component reproducing a reflection continuum associated with the Fe K line (the PEXRAV model in XSPEC). The illuminating power law is assumed to have a spectral index $\Gamma = 2$ with a high energy cutoff at 150 keV. Solar abundance and 60 deg inclination are assumed for the reflecting material. Moreover, the reflection continuum normalization is fixed such as to produce a Fe K line of about 1 keV above the reflection continuum. The major features of a reflection component, from cold irradiated material with significant optical depth, are a low ionization Fe K line with equivalent width of about 1 keV, a pronounced Fe K edge feature, a Compton hump around 20–30 keV, and a flat 2–10 keV continuum ($\Gamma \sim 0$) because of the internal photo-absorption.

Once the reflection continuum is added, we observe no significant changes in the quality of the fit (see the lower panel of Table 3). Nevertheless, the Fe K edge (being a predicted feature of the model) is not required anymore and the direct power-law emission has a steeper spectral index, consistent now with the values observed in AGNs (Ponti et al. 2006; Dadina 2007; Bianchi et al. 2009) and accreting Galactic sources (McClintock & Remillard 2006). Fe K bright MCs seem, thus, consistent with having a X-ray emission spectrum dominated by a strong reflection component.

Within the inner 15 arcmin from Sgr A*, massive MCs without significant neutral Fe Kα emission are also present (see Figure 2). The spectrum of the 50 km s^{-1} cloud is dominated by

the emission of Sgr A East, showing an intense (EW $\sim$ 1 keV) Fe K line at $\sim$6.66 keV. The line is relatively narrow ($\sigma = 70 \pm 2$ eV). Nevertheless, it shows small red and blue wings. Once the red wing is fitted with a narrow neutral Fe K line, we measure a Fe K intensity of $(1.65 \pm 0.11) \times 10^{-5}$ ph cm^{-2} s^{-1} (EW = 45 eV). It is not clear if this component is either tied to the SN remnant or to the 50 km s^{-1} cloud, for this reason we consider this as an upper limit on the emission from the 50 km s^{-1} cloud.

Also the 20 km s^{-1} cloud shows a prominent line at 6.66–6.7 keV. As in the 50 km s^{-1} cloud the neutral Fe K emission is weak with an intensity of about $(1.2 \pm 0.1) \times 10^{-5}$ ph cm^{-2}s^{-1} and an EW of $\sim$60 eV.

5. TIME-RESOLVED SPECTRAL ANALYSIS

5.1. Variations of the Fe K Line in the Bridge Region

The high statistics in the Fe K band, associated with the good spatial resolution and the long monitoring provided by *XMM-Newton*, allows the study of the Fe K line variations over the last eight years of observations. As shown in Table 1, several *XMM-Newton* pointings have short exposures and are close in time. In order to improve the statistics during those periods we summed the spectra of different observations close in time, as indicated in Table 1 which reports the grouping number for each observation. We, thus, obtained a significant measurement in 2002, one in March and one in 2004 November, moreover one in 2007 April, one in 2008 March and one in 2009 April.

In order to have a measurement of the Fe Kα intensity basically independent from continuum variations, we fit at each time the MC spectra with the phenomenological model composed of: WABS*(APEC+EDGE*(POWER-LAW+GAUS+GAUS)) instead of considering the more physical model including the reflection continuum component. We tested, however, that the same results can be obtained once the reflection continuum (tied to the Fe K line) is considered in the model. The Fe Kα line is, in fact, by far, the feature with the highest statistics of the spectrum, thus its intensity does not depend on the other components of the model.

We first fit the spectra of the different instruments separately. We obtain consistent results for all observations, thus we fit the spectra of the three instruments simultaneously. In the fit we assume that the Fe abundance, the hot plasma temperature, the column density of the neutral absorber, the depth of the absorbing edge, and the width of the Fe Kα line do not vary over time. We observe (as expected) that the intensity of the hot plasma emission is constant over time, thus we fix also this quantity.

We also observe that the spectral index of the power-law component is anti-correlated with the 4–10 keV flux. The spectral index becomes flatter at higher fluxes. This correlation is expected if the 4–10 keV continuum is composed of two components, a constant and steeper power-law component and a flatter one due to a variable reflection. Higher fluxes are thus associated with higher levels of reflection, and thus flatter spectra. This interpretation is reinforced by the evidence that this correlation is no longer significant once a reflection continuum tied to the Fe K line is added to the model. This suggests that the main 2–10 keV variations in these MCs are due to the variability of the reflection component.

Figure 5 shows the light curve of the intensity of the Fe K line in the bridge. This region experienced an increase of the Fe K line flux of a factor of about 2 in a few years. The fit of the light curve with a constant gives a $\chi^2 = 196.2$ for 5 dof,

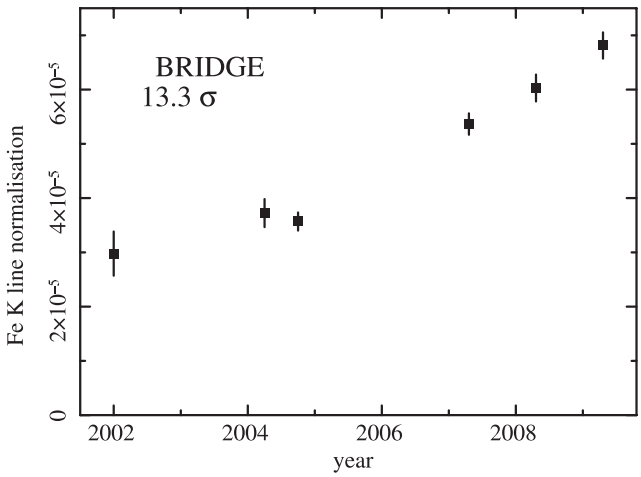

Figure 5. Fe K intensity light curve of the bridge region. Extremely significant variations (at a level of about 13.3σ) are occurring in this region. The main variations take place between 2006 and 2009.

corresponding to a significance of the variation of 13.3σ. The region of the bridge is spatially quite extended (see Figure 2), thus, in order to better constrain where the variation occurs, we divide the bridge in smaller regions as indicated by the green dashed ellipses in Figure 2. We identify the subregions with a progressive number (starting from west and anticlockwise) from 1 to 7.

Figure 6 shows the light curve of the first four subregions, while Figure 7 shows the variations of the regions from 5 to 7. The fit with a constant gives a $\chi^2 = 145.8, 89.9, 98.4, 15.4, 3.1, 4.8$, and 3.4 for 5 dof each, corresponding to a significance of the variation of 11.3σ, 8.6σ, 9.1σ, 2.6σ, 0.41σ, 0.78σ, and 0.46σ, for bridges 1, 2, 3, 4, 5, 6, and 7, respectively. Thus, the emission south of the bridge (in subregions 5, 6, and 7) is consistent with being constant, while highly significant variations of factors of about 3 are observed in the regions 1, 2, and 3. Interestingly the amplitude of the variations is similar in all the subregions from 1 to 3. We also note that all these regions (from bridge 1 to 4) have similar and significant line emission before the variation occurs, then not only a similar factor of variation, but also a similar intensity difference. Moreover, the peak of the variation occurs between 2005 and 2007 in bridge 1 (due to the lack of data it is difficult to establish it with precision), while the peak is reached in 2008 in bridge 2 and in 2009 in bridge 3. This suggests a lag between the variations in the different regions. This idea is reinforced by the similarity between the pattern of the variations in the three regions. A sharp rise of a factor of about 3 in the intensity of the Fe K line occurs in about three years, seen clearly in bridge 3 but consistent with bridge 2 and 1 trends. After the peak, the Fe K line intensity light curve shows either a stable period, or a very slow decay (see bridges 1 and 2). Also the light curve of bridge 4 fits in this scheme, if this region is just entering in the steep rise phase. The similar shape of the variations suggests a deep connection between these variations. In particular it indicates a common mechanism producing such behaviors that might be tied to the propagation of some event either inside or outside the MC. In this case, we foresee that the variations that occurred in the region "bridge 1" should propagate to bridges 2, 3, and 4 in the next years.

5.2. Variations of the Fe K Line in Other Molecular Structures

Figure 8 shows the light curve of MC1 and MC2. Over the decade of *XMM-Newton* observations, the Fe K line emission

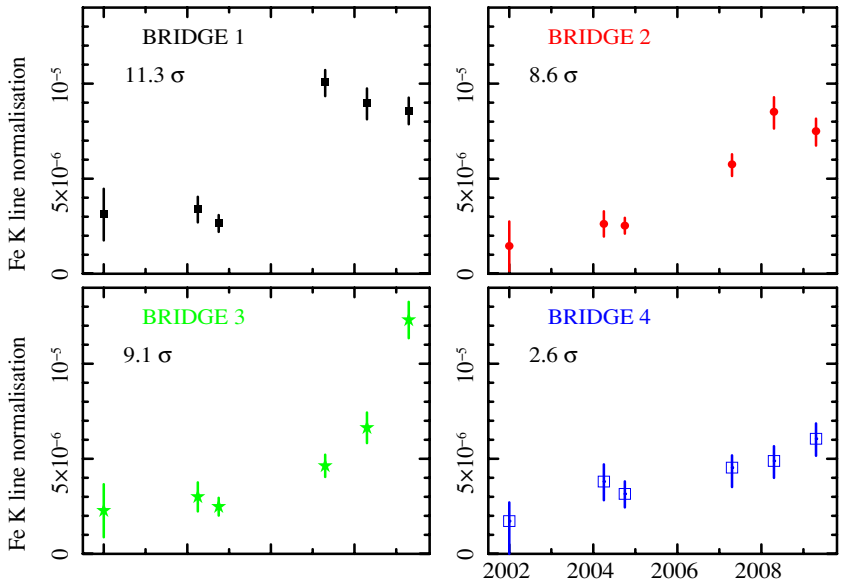

Figure 6. Fe K intensity light curves of the bridges 1, 2, 3, and 4 regions. Highly significant variations of the neutral Fe K line are seen in these regions. The variations have significance of 11.3σ, 8.6σ, 9.1σ, and 2.6σ for the bridges 1, 2, 3, and 4, respectively. In bridge 1 the peak of emission is reached between 2005 and 2007, in bridge 2 in 2008, and in bridge 3 in 2009. Surprisingly the different regions show similar amplitudes of variations (all about a factor of 3). The different light curves suggest they are undergoing a similar pattern of variations, with, after a quiet period, a fast rise of reflection intensity in about three years (see bridge 3) followed by either a stable or a decrease period of emission. In this scenario, bridge 4 might be just starting to rise.

(A color version of this figure is available in the online journal.)

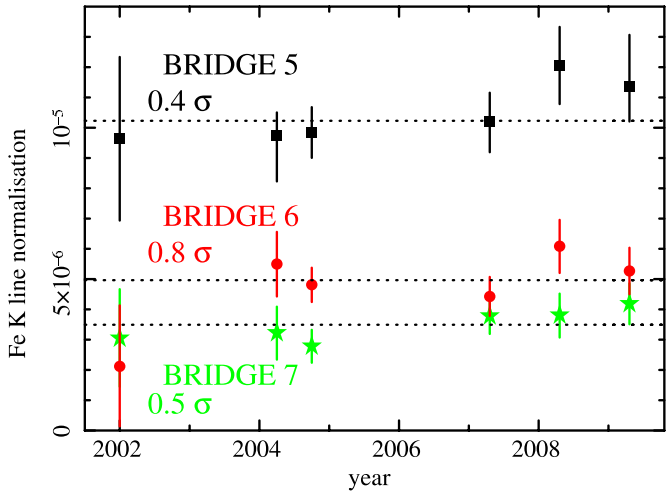

Figure 7. Fe K intensity light curve of the bridges 5, 6, and 7 regions. The reflection component from these regions is consistent with being constant between 2002 and 2009.

(A color version of this figure is available in the online journal.)

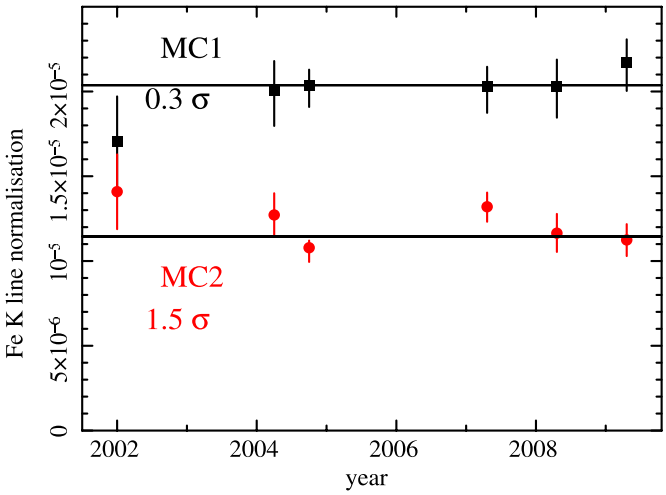

Figure 8. Fe K intensity light curves of MC1 and MC2. The emission from these MCs is consistent with being constant over the eight years *XMM-Newton* monitoring.

(A color version of this figure is available in the online journal.)

from these two MCs is constant. In fact, the best fit with a constant is satisfactory, giving a $\chi^2 = 2.6$ and 9.4 for 5 dof each, corresponding to a significance of the variation of the order of 0.3σ and 1.5σ for MC1 and MC2, respectively. We confirm the Muno et al. (2007) result of an overall constant Fe K emission coming from these MCs and we note that the spatial variability observed with *Chandra* might not appear here because of the lower spatial resolution. Unfortunately, the poor spatial resolution of the *Suzaku* telescopes does not permit a clear separation of the emission from MC1, MC2, and the bridge. The Fe K line variability claimed by Koyama et al. (2009) to come from feature 1 of Muno et al. (2007) might, instead, be produced in the bridge region. Figure 9 shows the light curve of G0.11-0.11. The Fe K emission is clearly variable, with a strong decrease of the order of 50% within the eight years of *XMM-Newton* monitoring. The fit with a constant gives a $\chi^2 = 24.2$ for 5 dof, corresponding to a significance of the variation of 3.8σ. The light curve suggests a linear decrease. Fitting the data with a linear relation the fit improves, giving now a $\chi^2 = 1.9$ for 4 dof, corresponding to a significant improvement of about 4.8σ.

6. TIME-RESOLVED IMAGES: DISCOVERY OF A SUPERLUMINAL ECHO IN AN X-RAY REFLECTION NEBULA

If, as indicated by the time-resolved spectral analysis, the variations in the different regions of the bridge are connected

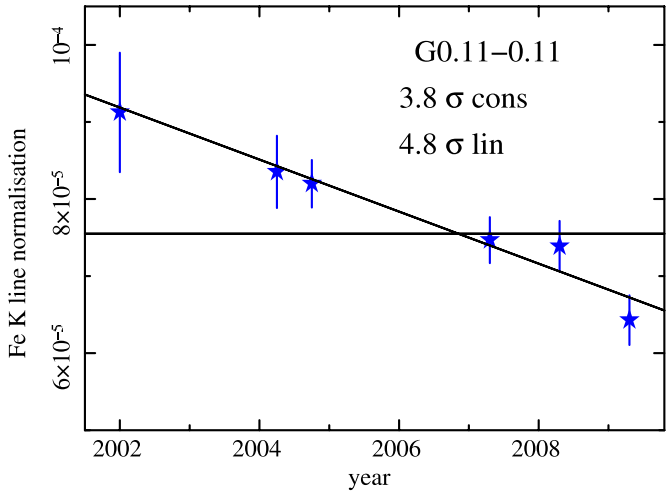

Figure 9. Fe K intensity light curve of G0.11-0.11. The reflection features in this MC are clearly variable (at a significance level of about 3.8σ) with a linear decay. A linear decrease is a better fit at 4.8σ level. A similar decline is shown by the Sgr B2 MC. The two MCs are consistent with reflecting the same Sgr A* flare (see the text for details).

(A color version of this figure is available in the online journal.)

and due to the propagation of an event inside the MC, the Fe K images between 2004 and 2009 should show the same variation and how it spatially had propagated. Figure 10 shows a progressive extension of the Fe K diffuse emission of the 2004 November, 2007 April, 2008 March, and 2009 April observations. The Fe K emission seems to evolve with time. The spot on the upper right corner of the image (MC 1) does not show clear intensity variations (the apparent different morphologies during the 2007, 2008, and 2009 observations are due to the presence of the EPIC-pn chip edge falling in the middle of the source during those pointings). On the other hand significant intensity variations appear in the positions traced by the dashed ellipses. During the 2004 observation, the bridge 1, 2, 3, and 4 regions are basically off and much fainter than MC1 and MC2. In 2007 bridge 1 lights up, becoming as intense as MC2. Bridge 2 also starts to rise, even if it does not reach its maximum yet. Further increase and evolution occurs in 2008. In 2009, it is bridge 3 that has the higher flux. The time behavior of the phenomenon suggests a connection/evolution in the intensity rise of the different regions. Nevertheless, we note that the emitting regions are causally disconnected. In fact, the delay time between the regions is of the order of 2–4 years, while they are separated by at least 15 light years on the plane of the sky, considering their projected distance and assuming that they are located at the distance of the GC.

7. DISCUSSION

The deep *XMM-Newton* monitoring of the 15 arcmin radius area around Sgr A* shows strong, diffuse, and complex pattern of Fe Kα emission from neutral or low-ionization ions. The Fe K radiation is asymmetrically distributed, being brighter along the Galactic plane and at positive galactic longitudes. In particular, a strong correlation between Fe K emitting regions and MCs is present, as already observed with other telescopes (Sunyaev et al. 1993; Murakami et al. 2000, 2001b; Yusef-Zadeh et al. 2007; Koyama et al. 2009).

The analysis of the *XMM-Newton* data confirms the presence of diffuse emission in this region and a correlation with MC. An attempt to separate the contribution from the different MC regions has been done using the CS maps provided by Tsuboi et al. (1999). We thus selected the regions shown in Figure 2 and performed a detailed spectral–temporal analysis. In particular, we analyzed the X-ray emission in the direction of G0.11-0.11, another region that we named "the bridge," plus two other MC regions (MC1 and MC2). We also analyzed the spectra of two massive MCs close to the GC, the 20 and 50 km s^{-1} MC (Coil et al. 2000).

The spectra of the Fe Kα bright MC suggest a reflection origin for this emission. The time-resolved spectral variability shows a complex pattern of variations, with some MCs increasing their Fe K emission, some decreasing, and some having a stable Fe K emission.

7.1. Superluminal Echo

Figure 10 shows the evolution of the illumination of the bridge region. In 2–5 years, we observe the progressive illumination of a region with projected angular size of about 1.92 arcmin. The studies of the CMZ through the different tracers (i.e., CS and ammonia) show that the bridge physical parameters are typical of the MC of the CMZ (Armstrong & Barrett 1985; Morris et al. 1983; Gusten et al. 1981; Tsuboi et al. 1999; Amo-Baladrón et al. 2009). Indeed the high line-of-sight velocity ($V_{\rm LSR} \sim 50$ km s^{-1}), the high internal temperature, and column density are consistent with the values observed in the CMZ. Moreover, Becklin et al. (1974) and Glass et al. (1987), studying the infrared images of the GC, argue that the bridge cannot be located closer to us than the GC, otherwise it would absorb the light coming from the numerous red stars located at the GC. Unlike the 20 and 50 km s^{-1} clouds, the bridge does not induce significant extinction in the stellar IR emission, suggesting a position behind Sgr A*.

Therefore, the projected angular size of 1.92 arcmin corresponds to a physical extent of at least 15 light years. The variation in the bridge implies, thus, a superluminal velocity of at least 4 times the velocity of the light. Figure 6 shows that the light curves of the different bridge regions show variations with similar factors, intensities and timescales, but each with a time delay. The observation of such variations cannot be due to the propagation of an event occurring inside the MC because it would have to travel faster than light (if the bridge is sitting on the plane of the sky). For the same reason it is also excluded that the observed variations are due to the propagation of low energy cosmic rays, produced within the MC. Moreover, both an internal and a nearby source can be excluded. In fact, whatever the bridge inclination is, the Fe K intensity variations must be decreasing with the square of the distance from the primary source. If the source is located either within the MC or nearby, this effect must produce, contrary to the observations, a high ratio between the intensity variations in the different regions. This, thus, indicates that the primary source is more distant than several times the bridge length. An internal or nearby source can be excluded also because of the lack of detection of transient sources, close enough to the bridge, within the period of the *XMM-Newton* monitoring. Either null or small delays are expected if the source is located inside, close or behind, the bridge.

It is also very unlikely that several different uncorrelated events happening within the MC (e.g., switching on of weak transients) can give rise to such a coherent pattern of time and spatial variations in causally disconnected regions.

Finally, it is interesting to note that in both 2004 observations all the bridge regions show significant Fe K emission,

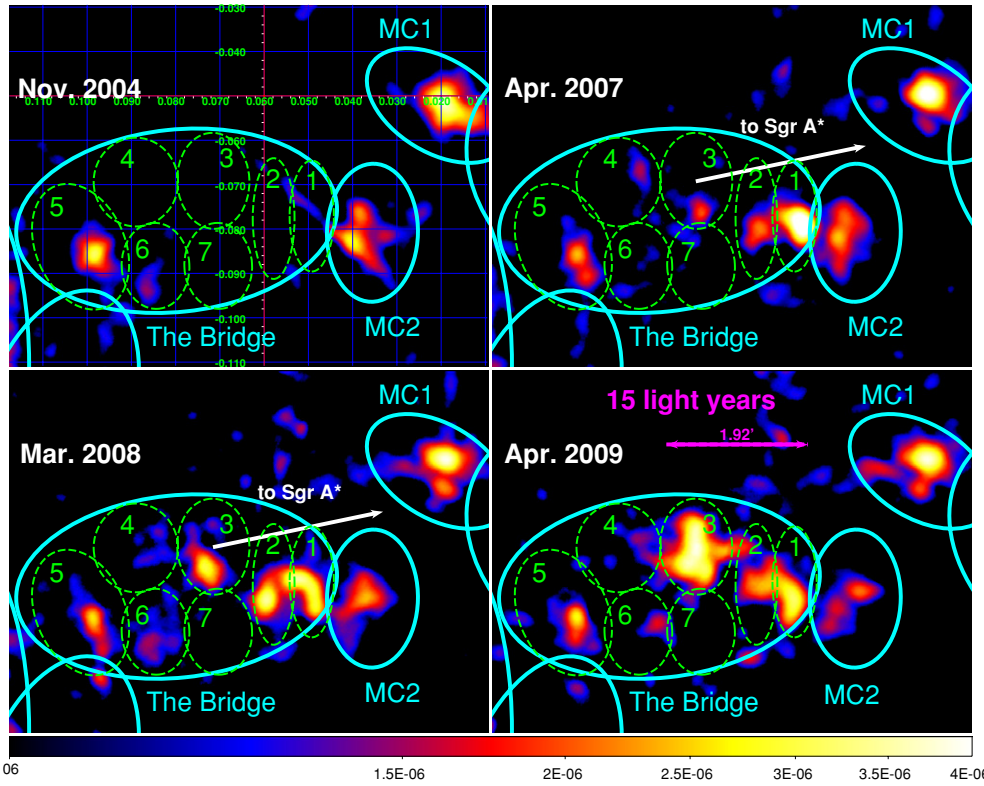

Figure 10. Fe Kα continuum-subtracted mosaic image of the different EPIC-pn observations of the bridge region. A brightening of the bridges 1, 2, 3, and 4 is clear. Such variation occurs in a time-scale of about 2–4 years, but in a spatial scale of about 15 light years. This apparent superluminal motion can be explained if the bridge MC is illuminated by a bright ($L > 1.3 \times 10^{38}$ erg s^{-1}) and distant (>15 pc) X-ray source active for several years. Either a flare from Sgr A* or a bright and long outburst of a X-ray binary can be the source of such a phenomenon. The observation of superluminal echo cannot be explained by either a single internal source or by low energy cosmic ray irradiation. It is also highly unlikely that the variations is produced by several uncorrelated sources.

even before the fast variations occur. This indicates that the bridge was an Fe K emitter even before that the superluminal variation occurred. A single burst from a primary source and a peculiar morphology of the reflecting material of the bridge might explain this behavior; nevertheless, most probably the primary source was active also before the superluminal variation occurred. This suggests that the source underwent a strong and fast short-time modulation, but within a longer lasting process.

In summary, the observation of the superluminal echo, the similar intensity Fe K variations in the different regions and the lack of detection of point source associated with it, imply that the origin of the variation has to be an external source, distant from the bridge. From the derived column density ($n_H = 9 \times 10^{22}$ cm^{-2}) and assuming a source distance of 18 pc (4 times the bridge dimension) we derive, to produce an Fe K line intensity of 1.1×10^{-5} ph cm^{-2} s^{-1}, a primary X-ray luminosity higher than 1.3×10^{38} erg s^{-1}, value close to the Eddington luminosity for a Solar mass BH.

Koyama et al. (1996), analyzing the X-ray emission from Sgr B2, suggested that the origin of the Fe K emission in that MC is due to a past flare of Sgr A*. Sgr B2 is an MC with a column density of 8×10^{23} cm^{-2} (see Table 2) and a radius of about 7 pc (Revnivtsev et al. 2004). Its projected distance is about 100 pc east of Sgr A* and a recent parallax measurement places it about 130 pc in front of the plane of Sgr A* (Reid et al. 2009). Figure 11 shows a sketch of the Galactic plane as seen from an observer above the Galaxy. The east of Sgr A* is presented with negative values and the Earth is located in the bottom of the figure at negative y-values. Sgr B2 is represented by the blue circle. Terrier et al. (2010) measured, in Sgr B2, an Fe K line intensity of 1.7×10^{-4} ph cm^{-2} s^{-1}. Assuming that the line is the echo of a past activity of Sgr A*, this implies an Sgr A* flare luminosity of $L \sim 1.4 \times 10^{39}$ erg s^{-1} terminating about 100 years ago.[8]

The direct implication of this scenario is, however, that the past activity of Sgr A* should light up other MCs. Are the emission and variations of the MC in the central 15 arcmin from Sgr A* consistent with such a scenario?

7.2. A Common Origin for the MC Emission and Variations: the Glorious Past of Sgr A Revealed by MC Emission?*

To evaluate this global scenario we have to take into account the properties of the different MCs. Table 2 shows the physical parameters of the MC under investigation. For most of the MC, the column densities have been measured through the integration of the CS emission.

As shown by the work of Amo-Baladrón et al. (2009), the n_H derived with this method can be overestimated by factors of the order of a few. In fact, this method is integrating the CS emission over the entire line of sight irrespective of the X-ray morphology. This technique might sum the contribution due to clouds having a similar line-of-sight velocity, but not associated with the cloud under investigation. Other sources of uncertainty are the CS/H abundances ratios and the CS excitation temperature. A more detailed study of the MC masses and distribution is beyond the scope of the present study, and it will be addressed in future works.

[8] We want to clarify that all along the paper we infer the history of the past activity of X-ray sources in the GC region without considering the lag due to the distance between the Earth and Sgr A*. This means that the Sgr A* flare would finish 100 years ago as seen from the Earth.

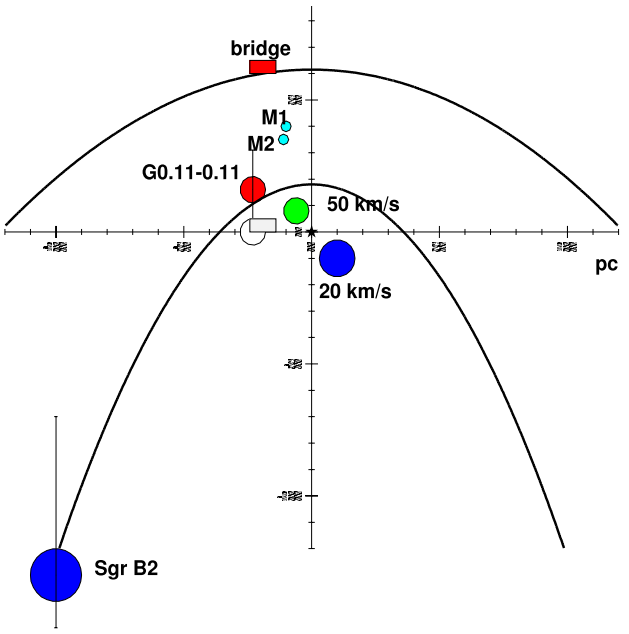

Figure 11. Sketch of the molecular face-on view of the Galactic plane as seen from the direction of the north Galaxy pole. Sgr A* is at the vertex indicated by a black star. Galactic east is toward negative abscissa and the direction toward the Earth is bottom, at negative ordinate. Sgr B2 is shown with a blue circle about 130 pc in front of Sgr A*. MC1 and MC2 are shown by the two light blue circles at 35 and 40 pc, respectively. The 20 and 50 km s^{-1} clouds are presented with blue and green circles. The bridge and G0.11-0.11 are shown with circles and rectangles, respectively. They are white when presented at the projected distance and red when their actual position is estimated. The parabola hitting Sgr B2 and G0.11-0.11 represents a light front emitted by Sgr A* 100 years ago, while the further parabola represents a light front emitted 400 years ago.

(A color version of this figure is available in the online journal.)

7.2.1. G0.11-0.11

The MC G0.11-0.11 (Tsuboi et al. 1997; Handa et al. 2006) is located between the Galactic Center Arc and Sgr A*, at Galactic coordinates $l = 0.^{\circ}108$, $b = -0.^{\circ}108$ (see Figures 2 and 11). The mass of this MC is highly debated in literature. The column density has been estimated through a detailed map in $H^{13}CO^+$ and in thermal SiO lines and the result is: $N(H_2) = (6–7) \times 10^{23}$ cm^{-2} (Handa et al. 2006), assuming that the $H^{13}CO^+(1–0)$ emission is thermalized. Nevertheless, Amo-Baladrón et al. (2009) showed it to be subthermally excited; their study of the CS maps indicates a lower column density of 5×10^{22} cm^{-2}. However, recently a detailed study of this MC indicates an even lower value of the column density, with $N_H = 2^{+1}_{-1.3} \times 10^{22}$ cm^{-2} (Amo-Baladrón et al. 2009); we assume this value for all the following calculations. G0.11-0.11 has a radius of 3.7 pc and a projected distance from Sgr A* of 25 pc. The strongest feature of the X-ray spectrum is the Fe K line at 6.4 keV. It has an intensity of 0.9×10^4 ph cm^{-2} s^{-1}. Assuming that the MC is located at its minimal distance from Sgr A* (see the white circle in Figure 11) and that the line is due to irradiation from it, the flare luminosity has to be $L \geqslant 10^{39}$ erg s^{-1} occurring more than 75 years ago (Sunyaev & Churazov 1998).

These values are surprisingly similar to the Sgr B2 ones. Moreover the light curve of both MCs is in a decay phase with about the same factors of variations (see Inui et al. 2009; Terrier et al. 2010; Figure 9). Assuming that G0.11-0.11 is produced by the same flare illuminating Sgr B2, it is possible to estimate the distance between Sgr A* and the cloud, and thus to measure the distance between G0.11-0.11 and the plane where Sgr A* is sitting. Thus, assuming a flare luminosity of 1.4×10^{39} erg s^{-1}, this implies that G0.11-0.11 is about 17 pc either in front or behind the plane of Sgr A* (red circle in Figure 11). To probe the hypothesis that G0.11-0.11 is responding to the same Sgr A* flare illuminating Sgr B2, we can apply another independent constraint. In fact, not only their column density, size, and Fe K intensities have to be linked, but also their distance with respect to Sgr A* has to be tied, in order to respond at the same time to the same flare. In other words, the position of G0.11-0.11 has to sit on the same illumination front hitting Sgr B2. Figure 11 shows that this is exactly the case, if we set G0.11-0.11 behind Sgr A*.

This is a strong constraint on the single flare hypothesis. It does not rule out other possibilities for the Fe K emission, but in those cases the observed ratios between line intensities, column densities, and distances must be such by coincidence. We also foresee a continuum correlation between the Sgr B2 and G0.11-0.11 light curves, at least if Sgr A* is the dominating source of illumination.

7.2.2. Other Constraints on the Recent-past Activity of Sgr A: the 20 and 50 km s^{-1} MCs*

Within 15 pc of Sgr A* there are two massive MCs, the 20 and 50 km s^{-1} clouds. Thanks to the interactions between these MCs and the material around them, it is possible to estimate the geometry of the region (Coil et al. 2000). In particular, the 50 km s^{-1} MC has a projected distance of about 5 pc from Sgr A* and seems to be about 5–10 pc behind it (Coil et al. 2000). Thus if a strong flare occurred in the recent past, this MC should still be reflecting its radiation. In Figure 11, the 50 and 20 km s^{-1} MCs are represented with the green and blue circles, respectively. The CS maps indicate, for the 50 km s^{-1} MC, a column density of about $n_H = 9 \times 10^{22}$ cm^{-2}. Thus, the upper limit on the neutral Fe K line places a limit on the mean luminosity produced by Sgr A* in the past 60–90 years (depending on the exact location), that is, $L \leqslant 8 \times 10^{35}$ erg s^{-1}. The study of Sgr B2, G0.11-0.11, the 20 and 50 km s^{-1} MC suggests, thus, that Sgr A* was in an active state about 100 years ago ($L \sim 10^{39}$ erg s^{-1}). Then, Sgr A* entered in a quiet period of low activity (with mean luminosity lower than several 10^{35} erg s^{-1}) until now. In this interpretation, we expect that the X-ray luminosity of Sgr B2 and G0.11-0.11, induced by Sgr A*, should be significantly lower in the next few decades.

7.2.3. The Bridge

As well as Sgr B2 and G0.11-0.11, the bridge is consistent with being illuminated by an external source but, opposite to the other MCs, its light curve shows a clear increase. Thus, these MCs cannot be seeing the same phase of the flare illuminating Sgr B2.

The observation of the apparent superluminal motion indicates an external illuminating source as the source of irradiation. As derived in Section 7.1, the source must have a luminosity higher than 1.3×10^{38} erg s^{-1}. This value is close to the Eddington luminosity for a stellar mass BH. We note that, although accretion onto a neutron star can reach even higher luminosity for short periods, it is improbable that it steadily produces such radiation for periods of years. On the other hand, a BH X-ray binary can produce such a luminosity for several years. However, the classical duty cycle of an X-ray binary outburst is a few months to years, thus we would expect modulations on

month timescales and a decrease of the Fe K emission in the next years. Further, deep X-ray observations of the field are thus mandatory to clarify this issue.

We also stress that we do not observe any bright enough X-ray source during the *XMM-Newton* monitoring around the bridge region. The brightest transient, active during the *XMM-Newton* monitoring and close to the bridge, is XMM J174554.4-285456, which has an estimated luminosity of about 2×10^{34} erg s^{-1}, not able to produce the observed variation. This implies that the delay between the arrival time of the primary and the reflected emission has to be significant. This excludes that the primary source is placed behind the cloud. Assuming that the maximal luminosity produced by a binary is of the order of 10^{39} erg s^{-1}, we can place an upper limit to its distance from the bridge of the order of 50 pc. We thus constrain the position of a possible binary responsible for the bridge variation to a distance between 18 and 50 pc from the bridge. Moreover, we note that (see Figure 10) the illumination starts to the Galactic west of the bridge and propagates toward the Galactic east, diffusing in the northern part of the bridge. This strongly suggests that the illuminating source is located east of the bridge, slightly north of it. This is the direction toward which Sgr A* is located.

The bridge might, in fact, be reflecting the light produced by an active period of Sgr A*. If the bridge is at its minimal distance from Sgr A* of about 18 pc, the flare luminosity should be $\sim 10^{38}$ erg s^{-1}. Assuming the same luminosity as seen by Sgr B2 and G0.11-0.11 of $L = 1.4 \times 10^{39}$ erg s^{-1}, we estimate the bridge location at about 60 pc behind the plane of Sgr A* (it cannot be in front because in that case the 50 km s^{-1} cloud should see the same flare). The location of the bridge about 60 pc behind Sgr A* is in agreement with the weak infrared absorption of the GC stars observed in the direction of the bridge (Güsten & Downes 1980; Glass et al. 1987). This position well behind Sgr A* is in agreement with an active phase of Sgr A* that lasted about 400 years.

7.2.4. MC1 and MC2

The two MCs called MC1 and MC2 have intense, but stable, Fe K emission. This confirms the result by Muno et al. (2007) who find a constant Fe K intensity coming from these regions. Nevertheless, the superb imaging capabilities of *Chandra* allowed the detection of changes in the shape of the emitting regions (Muno et al. 2007).

MC1 corresponds to the MC observed in ammonia and CO and called M0.02-0.05 by Armstrong & Barrett (1985). Due to its small line-of-sight velocity, the position of this MC is still debated. Nevertheless the strong Fe K emission and the broad molecular linewidths suggest a location within the CMZ for MC1. MC1 has a projected distance of 12.5 pc from Sgr A*, a column density of 4×10^{22} cm^{-2} (estimated using the CS maps), a radius of about 1.8 pc, and a Fe K line intensity of 2×10^{-5} ph cm^{-2} s^{-1}. As for the bridge, a flare from Sgr A* must have had a luminosity of about 7×10^{37} erg s^{-1} to illuminate MC1, if located at the projected distance. Again, arbitrarily assuming a Sgr A* flare luminosity of 1.4×10^{39} erg s^{-1} implies that MC1 must be about 50 pc behind Sgr A* (see the light blue circle in Figure 11).

In the position of the MC2 cloud there are no strong CS overdensities. We observe a CS flux corresponding to a column density of $n_H < 2 \times 10^{22}$ cm^{-2}. The projected distance of MC2 corresponds to 14 pc, the radius to 1.8 pc, and the line intensity to 1.2×10^{-5} ph cm^{-2} s^{-1}. Figure 11 shows that if MC2 is illuminated by the same flare of Sgr A* as Sgr B2, it should be located less than about 35 pc behind the supermassive BH. If this is the case, we predict that this MC should soon enter in the decay phase that Sgr B2 and G0.11-0.11 are experiencing now.

7.3. The Glorious (or Inglorious?) Past of Sgr A* Betrayed by MC

The X-ray emission from Sgr B2 and the 50 km s^{-1} MC indicate that the Sgr A* luminosity was lower than 8×10^{35} erg s^{-1} until 60–90 years ago, while it was brighter about 100 years ago with at least 10 years of nearly constant emission (with a luminosity of about 1.4×10^{39} erg s^{-1}).

The uncertainty on the position of the other MCs do not allow to derive strong constraints on the Sgr A* luminosity. Nevertheless, we can pose an upper limit to the distance between Sgr A* and these MCs of 200–300 pc (that correspond to the size of the CMZ). This immediately can be translated into an upper limit of the luminosity of Sgr A* in the last few thousand of years of $L \sim 10^{41}$ erg s^{-1}. This is in agreement with previous results obtained studying the X-ray emission from the MCs in the Galactic disc (Cramphorn & Sunyaev 2002). Thus, Sgr A*, even if brighter, did not reach accretion rates higher than $\eta \sim 10^{-5}$, the Eddington rate in the recent past.

In Figure 11, we estimated the MC positions arbitrarily assuming a Sgr A* luminosity of 1.4×10^{39} erg s^{-1} for many years. In reality Sgr A* might have had, in the past, many different flares with different peak luminosity (probably generated by accretion of cold stellar wind clumps; Cuadra et al. 2008), instead of one single period of activity. Only when the distance of the MC can be measured in an independent way will it be possible to safely estimate the luminosity of the Sgr A* activity and discriminate between these two scenarios. Nevertheless, a clue into this issue can be obtained through the comparison with similar BH accretion systems. The Sgr A* accretion rate implied by the Sgr B2 emission corresponds to the ones of the Galactic black holes (GBHs) in the transition between quiescence and low hard state. Assuming that the power spectral density of Sgr A*, at that accretion rate, is similar to one of the GBHs in the low hard state, with just the timescale of the variations scaled with the different BH mass, then for Sgr A* a low level of variations would be expected on a timescale longer than years (GBHs show little variability at frequencies lower than 0.01 Hz; Remillard & McClintock 2006). For this reason a long period of activity might be preferred to many strong flares. In this hypothesis, we would witness the rising phase (through the bridge) and the decay phase (through Sgr B2 and G0.11-0.11). In particular, the active phase of Sgr A* should have lasted about 400 years (implying a significant accretion duty cycle; Schawinski et al. 2010). This implies that a significant number of MCs should still be reflecting the Sgr A* radiation. In particular, assuming a uniform distribution of the MC within the CMZ and that the CMZ can be described by a disk with radius of 200 pc, it is possible to estimate (by computing the surface included between the two parabolas describing the beginning and the end of the flare) that nowadays we should observe about 30% of the MCs in the CMZ still reflecting Sgr A* emission. Interestingly, this value is of the same order of magnitude of the ratio between X-ray bright and weak MCs that can be roughly estimated from the comparison between the Fe K and molecular emission surveys of the CMZ (Yusef-Zadeh et al. 2007; Koyama et al. 1996). However, more detailed work is needed for a better estimate of this ratio and the comparison between different outburst models.

7.4. Alternatives to Sgr A*

The observation of a superluminal echo rules out either an internal source or cosmic rays as being responsible for the Fe K emission for the bridge. Moreover, the similarity between the Fe K intensity and MC physical properties of G0.11-0.11 and Sgr B2 suggests that an external X-ray source should have a luminosity of at least 10^{39} erg s^{-1} for many years and to be located close (a few parsecs) to the GC. If we assume a unique event to explain the Fe K luminosity of all the MCs, then the only possible alternatives to a flare from Sgr A* are either the passage of the shock generated by Sgr A East explosion onto the BH (Maeda et al. 2002; Rockefeller et al. 2005, but see Fryer et al. 2006), or the interaction between Sgr A East and the 50 km s^{-1} MC. Fryer et al. (2006) calculated, in fact, that the impact between the shock produced by the SN and the massive MC might have produced a luminosity up to about 10^{39} erg s^{-1} a few hundred years ago, with a considerably long period of activity.

Nevertheless the fast variability observed in the bridge region seems at odds with such a scenario. In fact between 2008 and 2009, the bridge 3 region increased its Fe K emission by a factor of 2. This implies that the emitting region must be smaller than about 0.3 pc. Therefore, dense matter clumps with light-years-scales must dominate the emission over an extended emission produced by the interaction between the 50 km s^{-1} MC and the Sgr A East shock. Moreover, the model reported in Fryer et al. (2006) predicts a slow decay of the emission produced by the Sgr A East shock. This might be difficult to reconcile with the factor of 2 decrease observed in G0.11-0.11 in eight years and the 4 order of magnitude decrease of the emission in the 50 km s^{-1} MC in only about 100 years. Thus, if only one source is illuminating all the MCs, then Sgr A* is the most probable candidate.

Nevertheless, we know that the GC region often experiences outbursts from transients. Some of these have high X-ray luminosity for a considerable amount of time and they may be placed in the correct position to highlight a nearby MC. At present, in fact, it cannot be excluded that the variation seen in the bridge region is due to an X-ray transient. However, a bright enough X-ray transient has never been observed close to the bridge, to G0.11-0.11, or to Sgr B2. In this interpretation, the transients should have been active before that the X-ray monitoring started. This implies that the illuminating sources must always be located in front of the MC, otherwise no big delay would be observed. Although possible, we think that this is unlikely.

As pointed out by Yusef-Zadeh et al. (2002, 2007) the X-ray bright MCs in the GC are very well correlated with the non-thermal radio emission. A distribution of low energy cosmic rays can produce low ionization Fe K lines with significant EW (of the order to 200–300 eV). Even if at present the Fe K emission from Sgr B2 and G0.11-0.11 is dominated by the radiation field produced by Sgr A*, it is important to continue to monitor those MCs because the prediction is that they should switch off in the near future. Then, the Fe K emission induced by the low energy electrons, if any are present, should persist, and become the dominating emission mechanism.

8. CONCLUSIONS

The deep *XMM-Newton* eight year monitoring of the Sgr A* region has allowed us to carry out a detailed study of the Fe Kα emission within the central 15 arcmin of the GC. We focused on the main emission features and reached the following conclusions.

1. The Fe Kα emission is asymmetrically distributed and is concentrated in features that are correlated to some high density MCs of the CMZ. These X-ray Fe K bright MCs show all the features of a reflection spectrum: neutral Fe K lines with EW of about 0.7–1 keV, Fe K edges ($\tau \sim 0.1$–0.3), and flat continua ($\Gamma \sim 0.6$–1.7).
2. We discovered an apparent superluminal motion corresponding to an MC called "the bridge." The illumination front spans at least 15 light years in a timescale of about 2–4 years. This phenomenon cannot be due to a source internal to the MC or to propagation of low-energy cosmic rays. A series of events is also unlikely because a similar pattern of variability is observed in causally disconnected regions. The most probable cause of this variation is the illumination of the molecular material from an external source. One possible geometry is that the illuminating fronts are nearly parallel to the bridge. To produce an apparent superluminal motion and the observed pattern of variations, the X-ray radiation must originate far away from the reflector (more than about 18 pc). The source must thus have had a luminosity higher than about 1.3×10^{38} erg s^{-1} for several years. A prediction of this picture is that the variations observed in the bridge region 1 propagate to region 2 and then 3 (maybe bridge region 4). Assuming that Sgr A* is the primary source and that it had a luminosity of about 10^{39} erg s^{-1}, it would place the bridge about 60 pc behind Sgr A*. This would imply either a long (about 400 years) or, to take intermittency to the extreme, it could imply that there have been multiple (i.e., two) brief events of activity of Sgr A* in the past.
3. We observe that the Fe K emission from G0.11-0.11 is decreasing, as if the MC is responding to the same flare that is illuminating Sgr B2, whose emission is also fading (Inui et al. 2009; Terrier et al. 2010). Considering the sizes and column density of the MC we estimate for G0.11-0.11 a position of about 17 pc behind Sgr A*, from the intensity of the Fe K line only. Surprisingly, in that position, G0.11-0.11 satisfies another completely independent constraint. In fact, it is consistent with being illuminated by the same light front hitting Sgr B2. These two MCs are, thus, experiencing the decay of a period of activity of Sgr A* (activity characterized by a luminosity of about 1.4×10^{39} erg s^{-1}) that lasted for at least 10 years (Revnivtsev et al. 2004) and that ended about 100 years ago (between 70 and 150 years ago). Other possibilities for the Fe K emission are not excluded, but in those scenarios the observed properties would result from pure chance.
4. The upper limit on the neutral Fe K emission from the 20 and 50 km s^{-1} MCs allows us to further constrain the mean level of activity of Sgr A* in the recent past, being lower than 8×10^{35} erg s^{-1} in the last 60–90 years. The Fe K emission from Sgr B2, G0.11-0.11 and the 50 km s^{-1} cloud suggest that the emission (presumably induced by Sgr A*) from Sgr B2 and G0.11-0.11 is destined to switch off in the next decades. At that point the emission produced by low energy cosmic rays, if present, might become dominant.
5. We also observe two bright MCs with intense but stable Fe K emission. Arbitrarily assuming that they reflect a flare of 10^{39} erg s^{-1}, they would be placed at about 35 and 40 pc behind Sgr A*.

6. The emission and variations of the MC in the central part of the Galaxy fit the scenario of a past period of activity of Sgr A* (either continuous or with bursts of emission). This period might have started a few hundreds of years ago and lasted until about 70–150 years ago. Since then, Sgr A* experienced a long period of low activity until now. This idea is in agreement with the observation of many Fe-K-bright MCs as well as many X-ray weak MCs and with the (poorly) known three-dimensional distribution of MCs within the CMZ.
7. The analysis of the long *XMM-Newton* monitoring of the GC shows that, in the past, Sgr A* had activity levels of the order of $\eta = 10^{-5}$ of its Eddington luminosity (as compared to its current $\eta = 10^{-8}$). In those conditions it appeared more similar to the classical low luminosity AGNs and the GBHs in the quiescent state. A deeper study of that period is important for the comprehension of the accretion mechanism, in view of the unification schemes.

Continuous deep X-ray monitoring of the region, as well as an improvement of the molecular maps of the CMZ are mandatory to fully understand the origin of the X-ray emission from the MC, in particular, to disentangle the contribution to the observed variations to be ascribed to the supermassive BH of the GC and to X-ray binaries of the region.

The connections between the X-ray Fe K maps, their variations and the measurements of the column densities and positions of the MC within the CMZ will allow to precisely reconstruct the history of the emission of Sgr A* and of the bright X-ray sources inside the CMZ. The flares from these sources will provide a tool to scan the CMZ and reconstruct the small-scale distribution of MC.

The work reported here is based on observations obtained with *XMM-Newton*, an ESA science mission with instruments and contributions directly funded by ESA Member States and NASA. The authors thank the referee Professor Mark Morris for the numerous comments that greatly helped to improve the paper. G.P. thanks ANR for support (ANR-06-JCJC-0047). G.P. also thanks M. Tsuboi for kindly providing the CS maps, and Anne Decouchelle, Vincent Tatischeff, Jesus Martin-Pintado Martin, Massimo Cappi, Stefano Bianchi, Matteo Guainazzi, Piergiorgio Casella, Kallmann Nagi, and Silvia Boscherini for useful discussion.

REFERENCES

Abbey, T., Carpenter, J., Read, A., Wells, A., XMM Science Centre, & Swift Mission Operations Center 2006, in The X-ray Universe 2005, ed. A. Wilson (ESA SP 604; Noordwijk: ESA), 943
Amo-Baladrón, M. A., Martín-Pintado, J., Morris, M. R., Muno, M. P., & Rodríguez-Fernández, N. J. 2009, ApJ, 694, 943
Armstrong, J. T., & Barrett, A. H. 1985, ApJS, 57, 535
Baganoff, F. K., et al. 2001, Nature, 413, 45
Bally, J., Stark, A. A., Wilson, R. W., & Henkel, C. 1987, ApJS, 65, 13
Becklin, E. E., Gatley, I., & Werner, M. W. 1982, ApJ, 258, 135
Becklin, E. E., Neugebauer, G., & Early, D. 1974, in Proc. 8th ESLAB Symp., H II regions and the Galactic Center, ed. A. F. M. Moorwood (Neuilly: ESRO), 227
Belmont, R., & Tagger, M. 2006, A&A, 452, 15
Bianchi, S., Bonilla, N. F., Guainazzi, M., Matt, G., & Ponti, G. 2009, A&A, 501, 915
Bykov, A. M. 2003, A&A, 410, L5
Coil, A. L., et al. 2000, ApJ, 544, L111
Cramphorn, C. K., & Sunyaev, R. A. 2002, A&A, 389, 252
Cuadra, J., Nayakshin, S., & Martins, F. 2008, MNRAS, 383, 458
Dadina, M. 2007, A&A, 461, 1209
de Grandi, S., & Molendi, S. 2009, A&A, 508, 565
Dogiel, V., et al. 2009, PASJ, 61, 901
Eisenhauer, F., Schödel, R., Genzel, R., Ott, T., Tecza, M., Abuter, R., Eckart, A., & Alexander, T. 2003, ApJ, 597, L121
Fryer, C. L., Rockefeller, G., Hungerford, A., & Melia, F. 2006, ApJ, 638, 786
Fukui, Y., Iguchi, T., Kaifu, N., Chikada, Y., Morimoto, M., Nagane, K., Miyazawa, K., & Miyaji, T. 1977, PASJ, 29, 643
Genzel, R., Schödel, R., Ott, T., Eckart, A., Alexander, T., Lacombe, F., Rouan, D., & Aschenbach, B. 2003, Nature, 425, 934
Ghez, A. M., Becklin, E., Duchjne, G., Hornstein, S., Morris, M., Salim, S., & Tanner, A. 2003, Astron. Nachr. Suppl., 324, 527
Ghez, A. M., et al. 2004, ApJ, 601, L159
Ghez, A. M., et al. 2005, ApJ, 635, 1087
Gillessen, S., Eisenhauer, F., Trippe, S., Alexander, T., Genzel, R., Martins, F., & Ott, T. 2009, ApJ, 692, 1075
Glass, I. S., Catchpole, R. M., & Whitelock, P. A. 1987, MNRAS, 227, 373
Goldwurm, A. 2008, in AIP Conf. Proc. 1085, High Energy Gamma-ray Astronomy, ed. F. A. Aharonian & F. Rieger (Melville, NY: AIP), 135
Goldwurm, A., Brion, E., Goldoni, P., Ferrando, P., Daigne, F., Decourchelle, A., Warwick, R. S., & Predehl, P. 2003, ApJ, 584, 751
Grevesse, N., & Anders, E. 1989, in AIP Conf. Proc. 183, Cosmic Abundances of Matter (Melville, NY: AIP), 1
Guainazzi, M., et al. 2010, A&A, submitted
Güsten, R. 1989, in IAU Symp. 136, The Center of the Galaxy, ed. M. Morris (Dordrecht: Kluwer), 89
Güsten, R., & Downes, D. 1980, A&A, 87, 6
Gusten, R., Walmsley, C. M., & Pauls, T. 1981, A&A, 103, 197
Handa, T., Sakano, M., Naito, S., Hiramatsu, M., & Tsuboi, M. 2006, ApJ, 636, 261
House, L. L. 1969, ApJS, 18, 21
Inui, T., Koyama, K., Matsumoto, H., & Tsuru, T. G. 2009, PASJ, 61, 241
Irvine, W. M., Goldsmith, P. F., & Hjalmarson, A. 1987, Interstellar Process., 134, 561
Jackson, J. M., Heyer, M. H., Paglione, T. A. D., & Bolatto, A. D. 1996, ApJ, 456, L91
Koyama, K., Inui, T., Matsumoto, H., & Tsuru, T. G. 2008, PASJ, 60, S201
Koyama, K., Maeda, Y., Sonobe, T., Takeshima, T., Tanaka, Y., & Yamauchi, S. 1996, PASJ, 48, 249
Koyama, K., Takikawa, Y., Hyodo, Y., Inui, T., Nobukawa, M., Matsumoto, H., & Tsuru, T. G. 2009, PASJ, 61, S255
Koyama, K., et al. 2007, PASJ, 59, 245
Maeda, Y., et al. 2002, ApJ, 570, 671
Makishima, K. 1986, in The Physics of Accretion onto Compact Objects, ed. K. P. Mason, M. G. Watson, & N. E. White (Lecture Notes in Physics 266; Berlin: Springer), 249
McClintock, J. E., & Remillard, R. A. 2006, in Compact Stellar X-ray Sources, ed. W. Lewin & M. van der Klis (Cambridge: Cambridge Univ. Press), 157
Melia, F., & Falcke, H. 2001, ARA&A, 39, 309
Molendi, S., & Gastaldello, F. 2009, A&A, 493, 13
Morris, M., Polish, N., Zuckerman, B., & Kaifu, N. 1983, AJ, 88, 1228
Morris, M., & Serabyn, E. 1996, ARA&A, 34, 645
Muno, M. P., Baganoff, F. K., Brandt, W. N., Park, S., & Morris, M. R. 2007, ApJ, 656, L69
Muno, M. P., et al. 2004, ApJ, 613, 1179
Murakami, H., Koyama, K., & Maeda, Y. 2001a, ApJ, 558, 687
Murakami, H., Koyama, K., Sakano, M., Tsujimoto, M., & Maeda, Y. 2000, ApJ, 534, 283
Murakami, H., Koyama, K., Tsujimoto, M., Maeda, Y., & Sakano, M. 2001b, ApJ, 550, 297
Nakajima, H., Tsuru, T. G., Nobukawa, M., Matsumoto, H., Koyama, K., Murakami, H., Senda, A., & Yamauchi, S. 2009, PASJ, 61, S233
Park, S., Muno, M. P., Baganoff, F. K., Maeda, Y., Morris, M., Howard, C., Bautz, M. W., & Garmire, G. P. 2004, ApJ, 603, 548
Ponti, G., Miniutti, G., Cappi, M., Maraschi, L., Fabian, A. C., & Iwasawa, K. 2006, MNRAS, 368, 903
Ponti, G., et al. 2009, MNRAS, 394, 1487
Porquet, D., Predehl, P., Aschenbach, B., Grosso, N., Goldwurm, A., Goldoni, P., Warwick, R. S., & Decourchelle, A. 2003, A&A, 407, L17
Reid, M. J., Menten, K. M., Zheng, X. W., Brunthaler, A., & Xu, Y. 2009, ApJ, 705, 1548
Remillard, R. A., & McClintock, J. E. 2006, ARA&A, 44, 49
Revnivtsev, M., Molkov, S., & Sazonov, S. 2006, MNRAS, 373, L11
Revnivtsev, M., Sazonov, S., Churazov, E., Forman, W., Vikhlinin, A., & Sunyaev, R. 2009, Nature, 458, 1142
Revnivtsev, M. G., et al. 2004, A&A, 425, L49
Revnivtsev, M. G., et al. 2007, A&A, 473, 857
Rockefeller, G., Fryer, C. L., Baganoff, F. K., & Melia, F. 2005, ApJ, 635, 441

Ryu, S. G., Koyama, K., Nobukawa, M., Fukuoka, R., & Tsuru, T. G. 2009, PASJ, 61, 751
Sakano, M., Warwick, R. S., & Decourchelle, A. 2006, J. Phys. Conf. Ser., 54, 133
Sakano, M., Warwick, R. S., Hands, A., & Decourchelle, A. 2004, Mem. Soc. Astron. Ital., 75, 498
Sawada, T., Hasegawa, T., Handa, T., & Cohen, R. J. 2004, MNRAS, 349, 1167
Schawinski, K., et al. 2010, ApJ, 711, 784
Schödel, R., et al. 2002, Nature, 419, 694
Sunyaev, R., & Churazov, E. 1998, MNRAS, 297, 1279
Sunyaev, R. A., Markevitch, M., & Pavlinsky, M. 1993, ApJ, 407, 606
Terrier, R., et al. 2010, ApJ, submitted
Tsuboi, M., Handa, T., & Ukita, N. 1999, ApJS, 120, 1
Tsuboi, M., Ukita, N., & Handa, T. 1997, ApJ, 481, 263
Valinia, A., Tatischeff, V., Arnaud, K., Ebisawa, K., & Ramaty, R. 2000, ApJ, 543, 733
Vollmer, B., Zylka, R., & Duschl, W. J. 2003, A&A, 407, 515
Wang, Q. D., Dong, H., & Lang, C. 2006, MNRAS, 371, 38
Yusef-Zadeh, F., Law, C., & Wardle, M. 2002a, ApJ, 568, L121
Yusef-Zadeh, F., Law, C., Wardle, M., Wang, Q. D., Fruscione, A., Lang, C. C., & Cotera, A. 2002b, ApJ, 570, 665
Yusef-Zadeh, F., Muno, M., Wardle, M., & Lis, D. C. 2007, ApJ, 656, 847